Interactions of the *Escherichia coli* DnaB–DnaC Protein Complex with Nucleotide Cofactors. 1. Allosteric Conformational Transitions of the Complex[†]

Anasuya Roychowdhury, **Michal R. Szymanski**, **Maria J. Jezewska**, and **Wlodzimierz Bujalowski**[*]

Department of Biochemistry and Molecular Biology, Department of Obstetrics and Gynecology, and The Sealy Center for Structural Biology and Molecular Biophysics, Sealy Center for Cancer Cell Biology, The University of Texas Medical Branch at Galveston, 301, University Boulevard, Galveston, Texas 77555-1053

Abstract

Interactions of nucleotide cofactors with both protein components of the *Escherichia coli* DnaB helicase complex with the replication factor, the DnaC protein, have been examined using MANT-nucleotide analogues. At saturation, in all examined stationary complexes, including the binary, DnaB–DnaC, and tertiary, DnaB–DnaC–ssDNA, complexes, the helicase binds six cofactor molecules. Thus, protein–protein and protein–DNA interactions do not affect the maximum stoichiometry of the helicase–nucleotide interactions. The single-stranded DNA dramatically increases the ATP analogue affinity, while it has little effect on the affinity of the NDP analogues, indicating that stationary complexes reflect allosteric interactions between the DNA- and NTP-binding site prior to the cofactor hydrolysis step and subsequent to product release. In the binary complex, the DnaC protein diminishes the intrinsic affinity and increases the negative cooperativity in the cofactor binding to the helicase; an opposite effect of the protein on the cofactor–helicase interactions occurs in the tertiary complex. The DnaC protein retains its nucleotide binding capability in the binary and tertiary complexes with the helicase. Surprisingly, the DnaC protein–nucleotide interactions, in the binary and tertiary complexes, are characterized by positive cooperativity. The DnaC assembles on the helicase as a hexamer, which exists in two conformational states and undergoes an allosteric transition, induced by the cofactor. Cooperativity of the allosteric transition depends on the structure of the phosphate group of the nucleotide. The significance of the results for the DnaB–DnaC complex activities is discussed.

Tight regulation of the DNA metabolism in both prokaryotes and eukaryotes involves specific multiprotein complexes, which provide intricate networks of regulation and control mechanisms (1–6). In the *Escherichia coli* cell, interactions between the primary replicative helicase DnaB protein and the essential replication factor DnaC protein are absolutely necessary for the initiation of the DNA replication at the origin of replication, oriC, as well as in the formation of the preprimosome, a multiprotein–DNA complex involved in priming the DNA synthesis, and in the restart of the stalled replication fork (1,7–11). Because the helicase is able to bind the single-stranded DNA (ssDNA)[1] with significant affinity, in the

[*]To whom correspondence should be addressed: Department of Biochemistry and Molecular Biology, The University of Texas Medical Branch at Galveston, 301 University Blvd., Galveston, TX 77555-1053. Telephone: (409) 772-5634. Fax: (409) 772-1790. wbujalow@utmb.edu.

absence of the DnaC protein, the replication factor is not necessary for the helicase to bind the nucleic acid (12–17). Rather, the DnaC allows the helicase to recognize the protein–nucleic acid complexes at the replication origin and the preprimosome and to engage in the next level of protein–protein–nucleic acid interactions (4,11).

Quantitative thermodynamic studies established that, in the presence of ATP analogue AMP-PNP or ADP, a maximum of six DnaC monomers bind with moderate intrinsic affinity to the DnaB hexamer (11). Moreover, the binding process is characterized by a significant positive cooperativity, with cooperative interactions limited to the two neighboring DnaC molecules. These data indicate that the DnaB–DnaC complex exists in vivo as a mixture of complexes with a different number of bound DnaC molecules, although the complex with six DnaC molecules bound dominates the distribution. Fluorescence energy transfer data indicate that, in solution, the DnaC protein-binding site is located on the large 33 kDa domain of the DnaB helicase (11). Electron microscopy studies have indicated a similar location of the bound DnaC protein molecules (18).

Activities of both the DnaB helicase and the DnaC protein are controlled by nucleotide cofactors (21–30). The DnaB hexamer possesses six nonspecific nucleotide-binding sites that can accept both NTP and NDP with similar affinities in stationary complexes, i.e., in the absence of the NTP hydrolysis (22–25). The binding is characterized by negative cooperative interactions between the adjacent sites, effectively splitting the binding process into two phases, with the first three nucleotides binding in the high-affinity phase and the three remaining nucleotides binding in the low-affinity phase (23,25). The two nucleotide binding phases seem to play a different role in the functioning of a hexameric helicase. Thus, studies of the analogous RepA hexameric helicase of plasmid RSF1010 indicate that the high-affinity phase is involved in the mechanical translocation process of the enzyme on the ssDNA and in the dsDNA unwinding (31). The DnaB helicase is a potent DNA-independent NTPase, with all six nucleotide-binding sites capable of performing the catalysis (23,25,32,33). On the other hand, the DnaC protein has only a single nucleotide-binding site, which exclusively binds adenosine nucleotides (26–30). Nevertheless, contrary to the DnaB helicase, the DnaC protein does not possess an intrinsic ATPase activity (26–30,34). Kinetic studies indicate that the DnaC protein exists in equilibrium between two conformational states prior to nucleotide binding, with ATP and ADP associating with the same conformation and with similar kinetic mechanisms (28,30).

Unwinding of the duplex nucleic acid, catalyzed by a helicase, requires binding and hydrolysis of nucleotide triphosphates (5,35–45). The enzyme performs a complex free energy transduction process, which is still not entirely understood for any helicase. On the level of the complex formation, the data indicate that the DnaC nucleotide-binding site is not involved in the stabilization of the DnaB–DnaC complex (11). The formation of the DnaB–DnaC complex is independent of the type of nucleotide bound to the helicase. Thus, the hydrolysis of NTP bound to the helicase is not required for the release of the DnaC protein from the complex, as previously thought (11). Moreover, the ssDNA bound to the helicase does not affect the DnaC protein binding. However, little is known about the effect of the formation of the DnaB–DnaC complex on the interactions of the helicase with the nucleotides. How interactions with the helicase affect the specific nucleotide binding to the DnaC protein and how the nucleotide binding controls the functional activities of the DnaB–DnaC complex are completely unknown.

---

[1]Abbreviations: NTP, nucleoside triphosphate; ADP, adenosine diphosphate; Tris, tris(hydroxymethyl)aminomethane; MANT-ADP, 3′(2′)-O-(N-methylanthraniloyl)adenosine 5′-diphosphate; MANT-ATP, 3′-O-(N-methylanthraniloyl)adenosine 5′-triphosphate; MANT-GDP, 3′(2′)-O-(N-methylanthraniloyl)guanosine 5′-diphosphate; GDP, guanosine diphosphate; AMP-PNP, β,γ-imidoadenosine 5′-triphosphate; ssDNA, single-stranded DNA; dsDNA, double-stranded DNA.

Quantitative understanding of the interactions of the DnaB–DnaC complex with nucleotide cofactors is an absolute prerequisite for formulation of any model of the activity of the replicative helicase and the replication factor. Such fundamental parameters of the interactions, like the maximum number of the nucleotides bound to the helicase in the binary DnaB–DnaC complex and tertiary DnaB–DnaC–ssDNA complex, i.e., the maximum number of subunits of the hexamer that are able to actively engage in nucleotide binding in these different complexes, the nature of the binding process, intrinsic affinities of the nucleotide-binding sites, and cooperativity, are still unknown. The number of DnaC molecules engaged in nucleotide binding, when the protein is bound in the binary and/or tertiary complexes with the helicase and the nucleic acid, intrinsic affinities, and the nature of these binding processes have never been addressed.

In this work, we present direct and extensive analyses of the binding nucleotide cofactors of both protein components of the binary, DnaB–DnaC, and tertiary, DnaB–DnaC–ssDNA, complexes. The data show that all six nucleotide-binding sites of the DnaB helicase can engage in interactions with the nucleotides in all the examined complexes. The presence of the ssDNA dramatically increases ATP analogue affinity, indicating that stationary complexes reflect allosteric interactions between the DNA- and NTP-binding sites. In the binary complex, the DnaC protein stabilizes the helicase–nucleotide complex in the most flexible conformational state, while the opposite is true for the tertiary complex. The DnaC hexamer, assembled on the helicase, undergoes a cooperative allosteric transition, which is controlled by cofactor binding.

MATERIALS AND METHODS

Reagents and Buffers

All chemicals were reagent grade. All solutions were made with distilled and deionized 18 MΩ (Milli-Q) water. The standard buffer, T4, is 50 mM Tris adjusted to pH 8.1 at 10 °C with HCl, 5 mM $MgCl_2$, 100 mM NaCl, 10% glycerol, and 1 mM DTT. ADP was from Sigma. MANT-ADP, MANT-ATP, and MANT-GDP analogues were synthesized and purified as previously described (22,24,25,46). The concentrations of the MANT-nucleotides were determined using an extinction coefficient (ε_{356}) of 5800 M^{-1} cm^{-1} (22,24,25,46).

DnaB Protein

The *E. coli* DnaB protein was purified as previously described by us (12,19,23,24). The concentration of the protein was spectrophotometrically determined using an extinction coefficient (ε_{280}) of 1.85×10^5 M^{-1} cm^{-1} (hexamer) (12,19,23,24).

DnaC Protein

The *E. coli* DnaC protein was purified as previously described by us (26–30). The concentration of the protein was spectrophotometrically determined using an extinction coefficient (ε_{280}) of 2.32×10^4 M^{-1} cm^{-1} (26–30).

Nucleic Acids

All ssDNA oligomers were from Midland. The concentrations of the labeled DNA oligomers have been spectrophotometrically determined (16,17,31,53).

Fluorescence Measurements

Steady-state fluorescence titrations were performed using the SLM-AMINCO 8100C instrument. To avoid possible artifacts, due to the fluorescence anisotropy of the sample,

polarizers were placed in excitation and emission channels and set at 90° and 55° (magic angle), respectively (32,33). The cofactor binding was monitored by following the fluorescence of the DnaB helicase free, or in the complex with the DnaC protein (λ_{ex}=300 nm; λ_{em}= 340 nm). Computer fits were performed using Mathematica (Wolfram, IL) and KaleidaGraph (Synergy Software, PA). All titration points were corrected for dilution and inner filter effects using the formula (23–25,46,47)

$$F_{i\text{cor}}=(F_i - B_i)\left(\frac{V_i}{V_\text{o}}\right) \times 10^{0.5b(A_{i\lambda_{ex}} + A_{i\lambda_{em}})}$$

(1)

where $F_{i\text{cor}}$ is the corrected value of the fluorescence intensity at a given point of titration, F_i is the experimentally measured fluorescence intensity, B_i is the background, V_i is the volume of the sample at a given titration point, V_o is the initial volume of the sample, b is the total length of the optical path of the sample expressed in centimeters, and $A_{i\lambda_{ex}}$ and $A_{i\lambda_{em}}$ are the absorbances of the sample at excitation and emission wavelengths, respectively (25). The relative fluorescence quenching, ΔF_{obs}, of the DnaB protein emission upon binding of the nucleotide cofactor is defined as $\Delta F_{obs}=(F_\text{o} - F_{i\text{cor}})/F_\text{o}$, where $F_{i\text{cor}}$ is the fluorescence of the protein at a given titration point and F_o is the initial value of the fluorescence of the sample (23–25).

In the case of the nucleotide binding to the DnaC protein, the nucleotide binding was monitored by following the fluorescence of the MANT-nucleotide analogue ($\lambda_{ex} = 356$ nm; $\lambda_{em} = 450$ nm) as a function of nucleotide concentration. All titration points were corrected for dilution and free MANT-nucleotide fluorescence, using the formula

$$F_{i\text{cor}}=(F_{iC} - F_{iN})\left(\frac{V_i}{V_\text{o}}\right) \times 10^{0.5b(A_{i\lambda_{ex}})}$$

(2)

where $F_{i\text{cor}}$ is the corrected value of the fluorescence intensity at a given point of titration, F_{iC} is the experimentally measured fluorescence intensity of the DnaC–MANT-nucleotide complex at a given titration point i, and F_{iN} is the corresponding fluorescence intensity of the free MANT-nucleotide analogue. The remaining symbols are the same as in eq 1. The analyzed spectroscopic signal (fluorescence) as a function of the fluorescing ligand concentration does not require normalization, with respect to the fluorescence of the free MANT-nucleotide (see below).

Quantitative Determination of Binding Isotherms and Stoichiometries of the DnaB Hexamer–Nucleotide Cofactor Complexes

The method for quantitatively estimating the total average degree of binding, $\Sigma\theta_i$ (the number of nucleotide molecules bound per DnaB hexamer), and the free nucleotide concentration, $[N]_F$, has been previously described in detail by us (14,47–50). Briefly, the experimentally observed ΔF_{obs} has a contribution from each of the different, possible i complexes of the DnaB hexamer with the cofactor. Thus, the observed fluorescence quenching is functionally related to $\Sigma\theta_i$ by

$$\Delta F_{obs}= \sum \Theta_i \Delta F_{i_{max}}$$

(3)

where $\Delta F_{i\max}$ is the molecular parameter characterizing the molar fluorescence quenching of the DnaB helicase with the nucleotide cofactor bound in complex i. The same value of ΔF_{obs}, obtainend at two different total helicase concentrations, P_{T_1} and P_{T_2}, indicates the same physical state of the enzyme; i.e., the total average degree of binding, $\Sigma\theta_i$, and the free nucleotide concentration, $[\mathrm{N}]_{\mathrm{F}}$, must be the same. The values of $\Sigma\theta_i$ and $[\mathrm{N}]_{\mathrm{F}}$ are then related to the total nucleotide concentrations, N_{T_1} and N_{T_2}, and the total protein concentrations, P_{T_1} and P_{T_2}, at the same value of ΔF_{obs} by

$$\sum \Theta_i = \frac{N_{\mathrm{T}_2} - N_{\mathrm{T}_1}}{P_{\mathrm{T}_2} - P_{\mathrm{T}_1}}$$

(4a)

$$[\mathrm{N}]_{\mathrm{F}} = N_{\mathrm{T}_x} - \left(\sum \Theta_i\right) P_{\mathrm{T}_x}$$

(4b)

where $x = 1$ or 2 (14,47–50).

Empirical Function Method

The DnaB hexamer has six nucleotide-binding sites, and each enzyme–nucleotide complex can exist in multiple conformational states, characterized by different molar fluorescence intensities. Thus, it is practically impossible to obtain independently all optical parameters for different complexes to fit the experimental fluorescence titration curves (25,48). However, this problem can be solved by introducing the representation of the observed quenching of the protein fluorescence, ΔF_{obs}, upon the binding of the nucleotides, as a function of the total average degree of binding, $\Sigma\theta_i$, via an empirical function (25,48). An empirical function, usually a polynomial, relates the experimentally determined dependence of the spectroscopic parameter (ΔF_{obs}) to $\Sigma\theta_i$ and is defined as

$$\Delta F_{\mathrm{obs}} = \sum_{j=0}^{n} \left(a_j \sum \Theta_i\right)^j$$

(5)

where a_j values are the fitting constants. The function defined by eq 5 is used to generate a theoretical isotherm for a binding model and to extract intrinsic binding parameters from the experimentally obtained single titration curve ([19],20,23,48,50,51).

Analytical Ultracentrifugation Measurements

Sedimentation velocity experiments were performed with an Optima XL-A analytical ultracentrifuge (Beckman Inc., Palo Alto, CA), using double-sector charcoal-filled 12 mm centerpieces. Sedimentation velocity scans were collected at the absorption band of the MANT moiety (356 nm) (19,30,31,53,55).

RESULTS

Binding of the Nucleotide Cofactor to the Free DnaB Helicase and to the Helicase in the Binary DnaB–DnaC Complex

Both components of the DnaB–DnaC complex bind nucleotide cofactors (see above) (22–30,33,34). However, the fact that the DnaC nucleotide-binding site accepts only adenine

nucleotides allows us to address the binding of the cofactors exclusively to the DnaB helicase, without any interference from the DnaC protein, using nucleotides with a different type of base than adenine (26,27). The DnaB protein has a preference for the purine nucleotides, with both guanosine and adenosine nucleotides binding with very similar affinities (25). However, binding of the unmodified nucleotide cofactors to the DnaB hexamer is not accompanied by a change in protein fluorescence that is adequate for performing quantitative analysis of the complex binding process. On the other hand, binding of the nucleotide analogues, e.g., MANT-GDP, is accompanied by a strong quenching of the protein fluorescence, providing an excellent signal for monitoring the association (19,25,46).

Fluorescence titrations of the DnaB protein with MANT-GDP, at two different protein concentrations and in the absence of the DnaC protein, in buffer T4 (pH 8.1 and 10 °C), are shown in Figure 1a. The maximum quenching of the protein fluorescence at saturation (ΔF_{max}) is 0.63 ± 0.03. The selected protein concentrations provide the separation of the binding isotherms up to the quenching value of ~0.5. Careful inspection of the spectroscopic titration curves, at a lower protein concentration, in Figure 1a indicates a complex binding process, with the presence of two binding phases and the titration curve extended over 3 orders of magnitude on the MANT-GDP concentration scale (25). To obtain a thermodynamically rigorous binding isotherm, independent of any assumption about the relationship between the observed signal and the degree of binding, $\Sigma\theta_i$, the fluorescence titration curves, shown in Figure 1a, have been analyzed, using the method outlined in Materials and Methods (47–50).

The dependence of the observed fluorescence quenching, ΔF_{obs}, upon the total average degree of binding, $\Sigma\theta_i$, of MANT-GDP on the DnaB protein is shown in Figure 1b. The separation of the binding isotherms allows us to obtained the values of $\Sigma\theta_i$ up to ~4 of the MANT-GDP molecules per DnaB hexamer. The plot in Figure 1b is clearly nonlinear, reflecting two binding phases. Association of the first three nucleotides induces a larger decrease in protein fluorescence emission than the binding of the subsequent three molecules of the cofactor. Extrapolation to the maximum quenching, ΔF_{max}, of 0.63 ± 0.03 shows that, at saturation, the DnaB hexamer binds 6.0 ± 0.5 molecules of MANT-GDP (23–25). The simplest statistical thermodynamic model that describes the nucleotide binding to the DnaB helicase is one in which the protein exhibits nearest-neighbor negative cooperativity among six otherwise identical nucleotide-binding sites (23–25, 48). This model, termed the hexagon model, has been previously used to analyze binding of nucleotides and DnaC protein molecules to the *E. coli* DnaB and plasmid RSF1010 RepA hexamers (23–25, 32, 50, 51). Thus, from the standpoint of the statistical thermodynamics, the DnaB hexamer is a small circular lattice with nearest-neighbor interactions. The partition functions for the hexagon model, Z_H, is then

$$Z_H = 1 + 6x + 3(3+2\sigma)x^2 + 2(1+6\sigma+3\sigma^2)x^3 + 3(3\sigma^2+2\sigma^3)x^4 + 6\sigma^4 x^5 + \sigma^6 x^6 \tag{6}$$

where $x = K[N]_F$, where K is the intrinsic binding constant and $[N]_F$ is the concentration of the free nucleotide. The total average degree of binding, $\Sigma\theta_i$, is then defined by the standard statistical thermodynamic formula (39)

$$\sum \Theta_i = \frac{\partial \ln Z_H}{\partial \ln [N]_F} \tag{7}$$

and

$$\sum \Theta_i = [6x + 6(3+2\sigma)x^2 + 6(1+6\sigma+3\sigma^2)x^3 + 12(3\sigma^2+2\sigma^3)x^4 + 30\sigma^4 x^5 + 6\sigma^6 x^6)]/Z_H$$

(8)

To directly analyze the spectroscopic titration curves in Figure 1a, using analytical eqs 6–8, one would have to know all of the molar fluorescence intensities of all possible DnaB–MANT-GDP complexes. As pointed out above, application of the empirical function approach allows us to avoid that problem(Materials and Methods) (23, 48, 50, 51). The plot of the observed fluorescence quenching, ΔF_{obs}, as a function of the total average degree of binding, $\Sigma\theta_i$, in Figure 1b is described by a second-degree polynomial function (eq 2) with coefficients a_1 (0.18653) and a_2 (−0.013452), respectively, as

$$\Delta F_{obs} = 0.18653\left(\sum \Theta_i\right) - 0.013452\left(\sum \Theta_i\right)^2$$

(9)

This function is then used to fit and generate theoretical titration curves for the binding of MANT-GDP to the DnaB hexamer, using the hexagon model, and to extract the intrinsic binding constant, K, and the cooperativity parameter, σ (48,50,51). The plot of the empirical function is included in Figure 1b. The solid lines in Figure 1a are the nonlinear least-squares fits of the experimental titration curves for binding of MANT-GDP to the DnaB hexamer, using eqs 6–9, with a single set of binding parameters, that provide an intrinsic binding constant K value of $(1 \pm 0.2) \times 10^6$ M^{-1} and a σ of 0.25 ± 0.05.

Fluorescence titration of the binary DnaB–DnaC complex with MANT-GDP is shown in Figure 2a. The concentrations of the helicase and the DnaC protein are 5×10^{-7} M(hexamer) and 5×10^{-6} M (monomer), respectively. At the selected concentrations of both proteins, the helicase is >95% saturated with the DnaC protein (11). For the sake of comparison, the analogous fluorescence titration of the DnaB protein alone with MANT-GDP, at the same enzyme concentration as in the complex, is also included in Figure 2a. The titration curve of the DnaB–DnaC complex is shifted toward higher nucleotide concentrations, indicating that the presence of the bound DnaC protein significantly diminishes the macroscopic affinity of the nucleotide for the helicase. In fact, the final plateau of the titration curve could not be reached in the experimentally available range of MANT-GDP concentrations. Notice, the high- and low-affinity binding phases are much more pronounced, as compared to the analogous binding phases observed for the free helicase, indicating much more pronounced negative cooperative interactions (see below).

We could not apply the same quantitative approach to determine the intrinsic binding constant and the cooperativity parameter, as described in the case of the free helicase, because the complex shows a tendency to precipitate at higher protein concentrations (Materials and Methods) (11). However, the presence of the same two binding phases and a very similar value of the protein fluorescence quenching for the high-affinity phase strongly suggest that the dependence of the observed fluorescence quenching upon the total average degree of binding is described by the same empirical function as obtained for the free enzyme (eq 9). The solid line in Figure 2a is the nonlinear least-squares fit of the experimental titration curve for binding of MANT-GDP to the DnaB hexamer in the DnaB–DnaC complex, using eqs 6–9, with a single set of binding parameters, that provide an intrinsic binding constant K of $(4 \pm 0.8) \times 10^5$ M^{-1} and a σ of 0.08 ± 0.02. Thus, the data indicate that, in the complex with the DnaC protein, at saturation, the DnaB helicase binds six MANT-GDP molecules. Nevertheless, the binding process is characterized by a

significantly lower intrinsic binding constant and profoundly strengthened negative cooperative interactions (see Discussion).

The binding of the nucleotide to the DnaB helicase in the DnaB–DnaC complex has been further examined using an independent sedimentation velocity approach (19,30,31,52,53). The MANT-GDP analogue has absorption bands with a maximum at ~356 nm, allowing us to monitor the sedimentation of the free cofactor and the DnaB–DnaC complex, without any interference from protein absorption (19,52,53). Sedimentation velocity scans of MANT-GDP (monitored at 356 nm) in the presence of the helicase–replication factor complex are shown in Figure 2b. The total concentrations of DnaB, DnaC protein, and MANT-GDP are 1×10^{-6} M (hexamer), 8×10^{-6} M, and 3×10^{-5} M, respectively. Analysis of the fluorescence titration curve in Figure 2a indicates that at the selected total concentrations of the nucleotide and the DnaB–DnaC complex we should observe ~4.1, of a maximum of 6 cofactor molecules, associated with the binary complex. At the applied rotational speed of 25000 rpm, the sedimentation boundary of the free MANT-GDP practically stays at the meniscus. The fast-moving boundary in Figure 2b corresponds to the DnaB–DnaC–MANT-GDP complex (37). From the total absorption of the initial scans (T), which corresponds to the total concentration of MANT-GDP, and the absorption of the boundary of free MANT-GDP (F), one can directly calculate the absorption of the MANT-GDP bound to the helicase in the binary complex as $C = T - F$. Thus, the concentration of the cofactor bound to the helicase is $C/T \times$ [MANT-GDP]$_T$. The total average degree of binding is then $\Sigma\theta_i = (C/T \times$ [MANT-GDP]$_T$)/[DnaB]$_T = 4.4 \pm 0.3$, in excellent agreement with the fluorescence titration data in Figure 2a.

Binding of the Nucleotide Cofactor to the DnaB Helicase Associated with the ssDNA

The DnaB helicase shows a significant affinity for the polymer ssDNA, with some preference for the adenosine polymers, only in the presence of ATP or ATP nonhydrolyzable analogues (12–20). However, we have found that binding of the ssDNA 20-mer, dA(pdA)$_{19}$, to the helicase, whose length corresponds to the site size of the enzyme–ssDNA complex, is characterized by the affinity, which allows us to address the nucleotide binding process for the enzyme–ssDNA complex [discussed in the companion paper (DOI 10.1021/bi9000529)]. Fluorescence titrations of the DnaB–dA(pdA)$_{19}$ complex with MANT-GDP, at two different protein concentrations, in buffer T4, are shown in Figure 3a. At the selected concentrations of the helicase and the ssDNA, 65% of the enzyme is initially saturated with the nucleic acid [discussed in the companion paper (DOI 10.1021/bi9000529]. The fact that a fraction of the helicase is still not saturated with the nucleic acid does not significantly affect the binding analysis. This is because at the selected protein and nucleic acid concentration binding of the DNA to the enzyme is a very fast process [discussed in the companion paper (DOI 10.1021/bi9000529)]. The affinity of the DNA for the helicase–ATP analogue complex is very high, and at such a large excess of the nucleic acid, any enzyme molecule with a bound cofactor will also be associated with the nucleic acid. The maximum quenching of the protein fluorescence at saturation is 0.61 ± 0.03, very similar to the value observed for the free enzyme (Figure 1a). The separation of the binding isotherms allowed us to obtain the values of the total average degree of binding, $\Sigma\theta_i$, up to ~5 of the MANT-GDP molecules per DnaB hexamer (Materials and Methods) (48,49).

The dependence of the observed fluorescence quenching, ΔF_{obs}, upon $\Sigma\theta_i$ of MANT-GDP on the DnaB protein is shown in Figure 3b. Extrapolation to the maximum quenching ($\Delta F_{max} = 0.61 \pm 0.03$) shows that, at saturation, the DnaB hexamer in the complex with the ssDNA binds 6.0 ± 0.3 molecules of MANT-GDP. The plot in Figure 3b has been analyzed using the empirical function approach (Materials and Methods) and can be described by a second-degree polynomial function (eq 2) with the following coefficients: $a_1 = 0.16701$, and $a_2 = -0.01084$ (Figure 3b). This empirical functional dependence of the observed relative

fluorescence quenching as a function of $\Sigma\theta_i$ was then used to fit and generate theoretical titration curves for the binding of MANT-GDP to the DnaB–ssDNA complex, using the hexagon model. The solid lines in Figure 3a are the nonlinear least-squares fits of the experimental titration curves for binding of MANT-GDP to the DnaB hexamer in the complex with the ssDNA, with a single set of binding parameters, that provide an intrinsic binding constant K of $(9 \pm 2) \times 10^5 \, M^{-1}$ and a σ of 0.4 ± 0.1. Thus, in the presence of the nucleic acid, the binding of six MANT-GDP molecules to the DnaB hexamer is characterized by an intrinsic affinity very similar to the values obtained for the free enzyme, but with lower negative cooperativity. Analogous experiments with MANT-ADP (data not shown) provided a K of $(9 \pm 2) \times 10^5 \, M^{-1}$ and a σ of 0.23 ± 0.06, which are very similar to the values observed in the absence of the DNA (25).

The situation is very different for the ATP analogue MANT-AMP-PNP. Fluorescence titrations of the DnaB–dA(pdA)$_{19}$ complex with MANT-AMP-PNP, at two different protein concentrations, in buffer T4, are shown in Figure 4a. The maximum quenching of the protein fluorescence at saturation is 0.45 ± 0.03. The separation of the binding isotherms allows us to obtain the values of the total average degree of binding, $\Sigma\theta_i$, up to ~3.9 MANT-AMP-PNP molecules per DnaB hexamer (Materials and Methods) (48, 49). Independent sedimentation velocity studies showed that a maximum of six AMP-PNP molecules bind to the enzyme in the complex with the ssDNA (data not shown). The dependence of the observed fluorescence quenching, ΔF_{obs}, on the $\Sigma\theta_i$ of the binding of MANT-AMP-PNP to the DnaB protein is shown in Figure 4b. The plot has been analyzed using the empirical function approach (Materials and Methods) and requires a third-degree polynomial function (eq 2) with the following coefficients: $a_1 = 0.07464$, $a_2 = -0.02957$, and $a_3 = 0.004931$ (Figure 4b). This empirical functional dependence of the observed relative fluorescence quenching as a function of $\Sigma\theta_i$ was then used to fit and generate theoretical titration curves for the binding of MANT-GDP to the DnaB–ssDNA complex, using the hexagon model. The solid lines in Figure 4a are the nonlinear least-squares fits of the experimental titration curves for the binding of MANT-AMP-PNP to the DnaB hexamer in the complex with the ssDNA, with a single set of binding parameters that provide an intrinsic binding constant K of $(5 \pm 1) \times 10^8 \, M^{-1}$ and a σ of 0.06 ± 0.1. It should be noted that the value of the intrinsic binding constant, K, may be even higher than this estimate because the initial part of the titration curves in Figure 4a is very close to the stoichiometric binding. Thus, in the presence of the nucleic acid, the binding of six MANT-AMP-PNP molecules to the DnaB hexamer is characterized by an intrinsic affinity larger by 3–4 orders of magnitude, as compared to the value of the same parameter obtained for the free enzyme (~$1 \times 10^5 \, M^{-1}$), but with similar negative cooperativity (25). Moreover, it is larger by 3–4 orders of magnitude than the intrinsic binding constant of the NDP analogues (see Discussion).

Binding of the Nucleotide Cofactor to the DnaB Helicase in the Tertiary DnaB–DnaC–ssDNA Complex

In the next set of experiments, we address the binding of the nucleotide cofactor to the DnaB helicase engaged in the tertiary complex with both the DnaC protein and the ssDNA. Fluorescence titrations of the DnaB–DnaC–dA(pdA)$_{19}$ complex with MANT-GDP, at two different sets of protein concentrations, are shown in Figure 5a. The striking feature of the plot in Figure 5a is a significantly lower maximum fluorescence quenching ($\Delta F_{obs}=0.35 \pm 0.02$) induced by the MANT-GDP binding, as compared to quenching observed for the helicase engaged only in the complex with the nucleic acid ($\Delta F_{obs} = 0.61 \pm 0.03$) (Figure 3a). Such a dramatic difference indicates that the simultaneous presence of the DnaC protein and the nucleic acid significantly affects the structure of the nucleotide-binding site of the helicase (see Discussion). Analysis of the titration curves in Figure 5a has been performed as described above, using the quantitative method outlined in Materials and Methods and the

empirical function approach (19, 48, 50, 51). The solid lines in Figure 5a are the nonlinear least-squares fits of the experimental titration curves for the binding of MANT-GDP to the DnaB hexamer engaged in the tertiary complex, with a single set of binding parameters, that provide an intrinsic binding constant K of $(2.1 \pm 0.4) \times 10^6$ M^{-1} and a σ of 0.5 ± 0.1. The presence of the DnaC protein increases the intrinsic affinity and slightly weakens the negative cooperative interactions in MANT-GDP binding, as compared to the DnaB hexamer associated only with the ssDNA (see Discussion).

The binding of the nucleotide to the DnaB helicase in the tertiary DnaB–DnaC–ssDNA complex has been further examined using the independent sedimentation velocity approach (see above). Sedimentation velocity scans of MANT-GDP (monitored at 356 nm) in the presence of the DnaB–DnaC–ssDNA complex are shown in Figure 5b. The total concentrations of DnaB, DnaC, ssDNA, and MANT-GDP are 1×10^{-6} M (hexamer), 8×10^{-6} M, 6.5×10^{-5} M, and 3×10^{-5} M, respectively. Analysis of the fluorescence titration curve in Figure 5a indicates that, at the selected total concentrations of the nucleotide and the DnaB–DnaC–ssDNA complex, we should observe ~5.6 of a maximum of 6 cofactor molecules, which can associate with the helicase. The fast-moving boundary in Figure 5b corresponds to the DnaB–DnaC–ssDNA–MANT-GDP complex. The analysis of these data has been performed as described above. The obtained total average degree of binding is $\Sigma\theta_i = (C/T \times [\text{MANT-GDP}]_T)/[\text{DnaB}]_T = 5.4 \pm 0.3$, in excellent agreement with the fluorescence titration data in Figure 5a (see Discussion).

Association of MANT-ADP with the DnaC Protein in the Absence and Presence of the ssDNA

So far, the experiments and analyses have concentrated on the DnaB component of the DnaB–DnaC complex. Recall that the nucleotide-binding site of the DnaC protein exclusively binds adenosine nucleotides (26–30). To examine the interactions of the DnaC protein with the cofactors, we selected a fluorescent analogue of ADP, MANT-ADP, whose binding to the DnaC protein is accompanied by a large increase in analogue fluorescence (26–30). Moreover, the affinity of the analogue for the DnaC nucleotide-binding site is indistinguishable from the affinity of the parent ADP. The DnaC protein has been reported to have some ssDNA affinity (54). Therefore, first, we address the effect of the ssDNA on the nucleotide binding to the protein.

Fluorescence titrations of the DnaC protein, alone and in the presence of two different concentrations of the ssDNA oligomer, dA(pdA)$_{19}$, with MANT-ADP in buffer T4, are shown in Figure 6. The largest fluorescence increase is observed for the free protein (26–30). Increasing the nucleic acid concentration systematically diminishes the observed fluorescence increase, providing a clear indication that the protein interacts with the nucleic acid. Nevertheless, the fact that the effect is not saturated, even at the highest nucleic acid concentration applied, 1.2×10^{-4} M (oligomer), indicates that in the affinity is characterized by a binding constant lower than ~10^4 M^{-1}. The solid lines in Figure 6 are the nonlinear least-squares fits of the experimental titration curves for the binding of MANT-ADP to the DnaC, free and in the presence of the ssDNA, using the single-site binding isotherm, defined as

$$F_{\text{obs}} = F_{\text{max}} \left(\frac{K_C [\text{N}]_F}{1 + K_C [\text{N}]_F} \right)$$

(10)

where F_{max}, is the maximum value of the observed fluorescence intensity at saturation, K_C is the binding constant, and $[\text{N}]_F$ is the free MANT-ADP concentration. The fits provide

excellent descriptions of the titration curves with binding constants (K_C) of $(3 \pm 0.6) \times 10^5$, $(9 \pm 2) \times 10^5$, and $(2.1 \pm 0.4) \times 10^6 \text{ M}^{-1}$ for the free protein and for the protein in the presence of the selected 20-mer concentrations. Thus, the increase in the nucleic acid concentration increases the intrinsic affinity of MANT-ADP for the nucleotide-binding site of the DnaC protein. Moreover, the diminished fluorescence increase of the bound analogue in the presence of the DNA indicates that the nucleic acid affects the structure of the nucleotide-binding site of the protein (see Discussion).

Stoichiometry and Intrinsic Affinity of MANT-ADP Binding to the DnaC Protein in the Binary Complex with the DnaB Helicase

Examination of the nucleotide binding to the DnaC protein in the complex with the DnaB protein requires careful considerations of the experimental design and the selected protein concentrations. MANT-ADP binds not only to the DnaC protein but also to the DnaB helicase (23,25–30). However, because GDP binds only to the helicase and not to the DnaC protein, one can exclusively monitor the binding of MANT-ADP to the replication factor, in the complex with the DnaB helicase, in the presence of 2 mM GDP, which blocks, to any detectable extent, the binding of the cofactor to the helicase, in the examined-MANT-ADP concentration range (11). We have previously determined the quantitative thermodynamics of the binding of DnaC to the DnaB hexamer under these conditions (11). At saturation, six DnaC protein molecules bind to the helicase with moderate intrinsic affinity and positive cooperative interactions. In other words, there is a distribution of complexes with different numbers of bound DnaC protein molecules. Nonetheless, the complex with six DnaC molecules bound to the enzyme dominates the distribution at physiological concentrations of the DnaC protein (11). Moreover, it can be formed in solution as a single, defined entity, amenable to analytical analysis, while complexes with different numbers of bound DnaC molecules cannot (11). Thus, we are interested in the situation in which as much of the DnaC protein as possible is bound to the helicase and, mostly, in a single type of complex, i.e., with six DnaC protein molecules bound. One also has to take into account the fact that the complex shows a tendency to precipitate at a high protein concentration (see above). The optimal concentration of the DnaB protein is then 1×10^{-6} M (hexamer).

The partition function, Z_H, which describes the DnaC binding to the DnaB helicase, is defined by the expression analogous to eq 6 (11,48,50,51). Therefore, knowing the intrinsic binding constant and the cooperative interaction parameter, one can obtain the distribution of all possible complexes of the helicase with a different number of bound DnaC molecules, C_1, C_2, C_3, C_4, C_5, and C_6, at the selected enzyme concentration, as a function of the total DnaC concentration, using the formulas

$$C_1 = \frac{6K[\text{DnaC}]_F}{Z_H}$$

(11a)

$$C_2 = \frac{3(3+2\sigma)K^2[\text{DnaC}]_F^2}{Z_H}$$

(11b)

$$C_3 = \frac{2(1 - 6\sigma + 3\sigma^2)K^3[\text{DnaC}]_F^3}{Z_H}$$

(11c)

$$C_4 = \frac{3(3\sigma^2 + 2\sigma^3)K^3[\text{DnaC}]_\text{F}{}^4}{Z_\text{H}}$$

(11d)

$$C_5 = \frac{6\sigma^4 K^5[\text{DnaC}]_\text{F}{}^5}{Z_\text{H}}$$

(11e)

$$C_6 = \frac{\sigma^6 K^6[\text{DnaC}]_\text{F}{}^6}{Z_\text{H}}$$

(11f)

The plots of the distribution of the different DnaB–DnaC complexes are shown in Figure 7. The plots were generated using eqs 11a–11f, with an intrinsic binding constant K of 2×10^5 M^{-1} and a cooperative interaction parameter ($\sigma \approx 30$), corresponding to the parameters determined for the DnaC protein binding to the helicase in the presence of 2 mM GDP (11). It is evident that, at the total DnaB protein concentration of 1×10^{-6} M (hexamer), the complex with six DnaC molecules bound begins to dominate the distribution at a $[\text{DnaC}]_\text{T}$ of $>4 \times 10^{-6}$ M.

The molar fraction of the total DnaC concentration bound to the helicase, C_B, at a given total DnaB concentration, $[\text{DnaB}]_\text{T}$, and at any $[\text{DnaC}]_\text{T}$, is defined by the expression

$$C_\text{B} = \frac{(\sum \Theta_i)[\text{DnaB}]_\text{T}}{Z_\text{H}}$$

(12)

The plot of the molar fraction of C_B as a function of the total DnaC concentration, $[\text{DnaC}]_\text{T}$, is included in Figure 7. For the selected total DnaB concentration [1×10^{-6} M (hexamer)], the required total DnaC concentration is $\approx 5 \times 10^{-6}$ M, at which $>95\%$ of the total population of the DnaC protein in the sample is associated with the DnaB helicase, in the complex containing six DnaC molecules.

Fluorescence titration of the DnaC protein in the complex with the DnaB helicase, with MANT-ADP, in buffer T4, containing 2 mM GDP, is shown in Figure 8a. For the sake of comparison, the fluorescence titration of the free DnaC protein at the same replication factor concentration is included in Figure 8a. The macroscopic affinity of the cofactor for the DnaC protein and the maximum fluorescence increase accompanying the binding to the protein in the binary DnaB–DnaC complex are higher than those observed for the free protein. The maximum number of DnaC protein molecules engaged in the complex with MANT-ADP, when the protein is in the binary complex with the DnaB helicase, has been addressed using the sedimentation velocity approach (see above). Sedimentation velocity scans of MANT-ADP (monitored at 356 nm), in the presence of the DnaB–DnaC complex and 2 mM GDP, are shown in Figure 8b. The total concentrations of DnaB, DnaC, and MANT-ADP are 1×10^{-6} M (hexamer), 5×10^{-6} M, and 3×10^{-5} M, respectively. At selected total concentrations, we should observe maximum saturation of the DnaC protein (Figure 8a). The fast-moving boundary in Figure 8b corresponds to the DnaB–DnaC–MANT-ADP complex (52, 53). Applying the same analysis of these data, as described above, the obtained, total average degree of binding of MANT-ADP per DnaC protein is $\Sigma\theta_i$

= ($C/T \times$ [MANT-ADP]$_T$)/[DnaC]$_T$=0.96 ± 0.15, indicating all the DnaC protein molecules, bound to the helicase, are engaged in the complex with the nucleotide (see Discussion).

Once the maximum stoichiometry of the binding of MANT-ADP to the DnaC protein in the complex with the DnaB helicase has been established, we can address the affinity of the nucleotide. The most striking feature of the plot in Figure 8a is an apparent positive cooperativity evident in the sigmoidal initial part of the titration curve. Notice that the plot is shown on a linear scale with respect to nucleotide concentration (48). The dashed line in Figure 8a is the nonlinear least-squares fit of the experimental titration curve, assuming that each nucleotide-binding site on the bound DnaC protein is completely independent, using eq 10. However, the independent-site binding model does not provide adequate representation of the titration curve. Thus, six DnaC molecules bound to the DnaB hexamer cannot be treated as independent nucleotide-binding units (see Discussion).

Kinetic studies revealed that the DnaC protein exists in an equilibrium between two conformations prior to nucleotide binding (27,28,55). Only one conformation of the DnaC protein has the ability to bind nucleotide cofactors. The simplest extension of these results to the behavior of six DnaC molecules in the binary complex with the DnaB helicase is to assume that the bound DnaC proteins exist in an equilibrium of two conformations, when bound to the helicase, with only one conformation capable of binding the cofactors. Binding of the cofactor to one DnaC molecule induces the transition of all bound molecules into the conformation, which binds the cofactor. In other words, six bound DnaC molecules behave like an allosteric hexamer, described by the Monod–Wyman–Changeux (MWC) model (56). The communication between the DnaC molecules in such an allosteric hexamer, assembled on the DnaB helicase, would be mediated through cooperative interactions between the DnaC molecules, each molecule constituting the subunit of the assembled hexamer (11).

The partition function of the considered variant of the allosteric MWC model, Z_A, with only one conformation of the DnaC hexamer, assembled on the DnaB helicase, binding the nucleotide cofactor, is defined by

$$Z_A = 1 + K_A (1 + K_{MC} [N]_F)^6 \tag{13}$$

where K_A is the allosteric constant characterizing the conformational transition of the assembled hexamer of the bound DnaC molecules and K_{MC} is the intrinsic binding constant of the cofactor for the conformation of the DnaC hexamer, which binds the cofactor. The total average degree of binding, $\Sigma\theta_{Ai}$, is then defined by

$$\sum \Theta_{Ai} = \frac{6 K_{MC} [N]_F [K_A (1 + K_{MC} [N]_F)^5]}{1 + K_A (1 + K_{MC} [N]_F)^6} \tag{14}$$

The observed fluorescence increase, F_{obs}, is then

$$F_{obs} = F_{max} [DnaB]_T \left(\sum \Theta_{Ai} \right) \tag{15}$$

The maximum value of the fluorescence increase, F_{max}, can be estimated from the titration curve in Figure 8a. The solid line in Figure 8a is the nonlinear least-squares fit of the

experimental titration curve for MANT-ADP binding to the six DnaC molecules, assembled as a hexamer in the complex with the DnaB helicase, using eqs 13–15, with two fitting parameters, K_{MC} and K_A. It provides an intrinsic binding constant K_{MC} of $(7.1 \pm 1.4) \times 10^5$ M^{-1} and an allosteric constant K_A of 0.1 ± 0.03. It is clear that the model furnishes an excellent description of the experimental titration curve (see Discussion).

Stoichiometry and Affinity of MANT-ADP Binding to the DnaC Protein Engaged in the Tertiary DnaB–DnaC–ssDNA Complex

Fluorescence titrations of the DnaC protein in the tertiary DnaB–DnaC–dA(pdA)$_{19}$ complex, with MANT-ADP, in buffer T4, containing 2 mM GDP, are shown in Figure 9a. For the sake of comparison, the fluorescence titration of the same DnaB–DnaC complex, in the absence of the ssDNA, is also included in Figure 9a. There is a clear increase in the fluorescence emission of the analogue, accompanying the binding to the DnaC protein in the tertiary complex with the helicase and the ssDNA, as compared to the binary DnaB–DnaC complex (Figure 8a), indicating that the structure of the nucleotide-binding site of the DnaC protein is differently affected by interactions with the enzyme associated with the nucleic acid (see Discussion). The maximum number of the DnaC protein molecules, engaged in the complex with MANT-ADP, when the protein is in the tertiary complex has been determined, using the independent sedimentation velocity approach, analogously as described above. Sedimentation velocity scans of MANT-ADP (monitored at 356 nm), in the presence of the DnaB–DnaC–ssDNA complex and 2 mM GDP, are shown in Figure 9b. The total concentrations of DnaB, DnaC, ssDNA, and MANT-ADP are 1×10^{-6} M (hexamer), 5×10^{-6} M, 6.5×10^{-5} M, and 3×10^{-5} M, respectively. At the selected total concentrations of the helicase, DnaC, and nucleic acid, we should observe maximum saturation of the DnaC protein (Figure 9a). Applying the same approach, as discussed above, the total averaged degree of binding $\Sigma\theta_i = (C/T \times [\text{MANT-ADP}]_T)/[\text{DnaC}]_T = 0.95 \pm 0.15$, indicates that all DnaC protein molecules in the tertiary complex can engage in interactions with the cofactor (see Discussion).

Having established the maximum stoichiometry of binding of MANT-ADP to the DnaC protein in the complex with the DnaB helicase, one can address the affinity of the nucleotide. The apparent cooperativity, already seen in the binary complex (Figure 8a), is now much more pronounced. The solid line in Figure 9a is the nonlinear least-squares fit of the experimental titration curve using the MWC model, as defined by eqs 13–15, with two fitting parameters, K_{MC} and K_A (56). The fit provides an intrinsic binding constant K_{MC} of $(7.9 \pm 1.9) \times 10^5$ M^{-1} and an allosteric constant K_A of 0.005 ± 0.001. There is excellent agreement between the experimental and theoretical curves. Although the intrinsic binding constant, K_{MC}, is only modestly increased, the data indicate that the presence of the ssDNA in the tertiary complex dramatically shifts the conformational equilibrium of the bound DnaC protein toward the conformation that does not bind the ADP analogue, as compared to the binary DnaB–DnaC complex (see Discussion).

Simultaneous Binding of MANT-ADP to Both Protein Components of the Tertiary DnaB–DnaC–ssDNA Complex

In the experiments described above, we have examined the exclusive binding of the nucleotide cofactors to one of the protein components of the DnaB–DnaC complex in different systems. In the next set of experiments, we address the extent to which these two binding processes are independent, by examining the simultaneous binding of MANT-ADP to both the DnaB and DnaC protein in the tertiary DnaB–DnaC–ssDNA complex. This is the most challenging arrangement of all systems we have examined so far. Fluorescence titrations of the tertiary DnaB–DnaC–dA(pdA)$_{19}$ complex, with MANT-ADP, in buffer T4, at two different sets of protein concentrations, are shown in Figure 10a. At selected DnaB

and DnaC concentrations, the helicase is >95% saturated with the DnaC protein (Figure 7). Notice that in this experiment the binding of the cofactor to the tertiary complex is observed through the helicase, as only the association of MANT-ADP with the DnaB protein is accompanied by the quenching of the tryptophan emission. Thus, the value of $\Sigma\theta_i$ is exclusively determined only for the helicase. Nevertheless, the binding of the nucleotide to both proteins is thermodynamically linked by the free concentration of the cofactor, allowing us to address binding of the cofactor to both protein components of the tertiary complex (see below).

The separation of the titration curves provides the value of the total average degree of binding, $\Sigma\theta_i$, up to ~3.7 (ΔF_{obs} ~ 0.2). The dependence of the observed fluorescence quenching, ΔF_{obs}, on $\Sigma\theta_i$ is shown in Figure 10b. The data in Figure 10b have been analyzed using the empirical function approach (Materials and Methods) and using the fact that, from Figure 10a, we know the maximum value of the DnaB protein quenching at saturation with the cofactor (ΔF_{max}=0.52±0.03). The required function is a third-degree polynomial (eq 2) with the following coefficients: a_1=0.07716, a_2=−0.02442, and a_3=0.004355. As we pointed out, the system is extremely complex. The DnaB helicase is almost completely saturated with the DnaC protein. Part of the DnaC protein is bound to the DnaB helicase, forming an allosteric hexamer. However, part of the DnaC protein is free, i.e., not bound to the helicase and interacting with the ssDNA (see above). Therefore, there are three components of the system, which must be considered. The partition function of the entire system, Z_S, is then

$$Z_S = Z_H + Z_A + K_C[N]_F \tag{16}$$

where Z_H is the part that describes the binding of MANT-ADP to the DnaB hexamer in the tertiary complex, Z_A is the part that describes the binding of the nucleotide to the DnaC allosteric hexamer in the tertiary complex, $K_C[N]_F$ is the part that characterizes the binding of the cofactor to the free DnaC protein, in the presence of the ssDNA, at the selected nucleic acid concentration, and $[N]_F$ is the free concentration of MANT-ADP. Therefore, the total partition function, Z_S, is defined as

$$\begin{aligned}
Z_S = {} & 1 + 6K[N]_F \\
& + 3(3 \\
& + 2\sigma)K^2[N]_F{}^2 \\
& + 2(1 + 6\sigma + 3\sigma^2)K^3[N]_F{}^3 \\
& + 3(3\sigma^2 \\
& + 2\sigma^3)K^4[N]_F{}^4 \\
& + 6\sigma^4 K^5[N]_F{}^5 \\
& + z\sigma^6 K^6[N]_F{}^6 \\
& + K_A(1 + K_{MC}[N_F])^6 \\
& + K_C[N]_F
\end{aligned} \tag{17}$$

The total average degree of binding of MANT-ADP on the DnaB helicase in the system, $\Sigma\theta_{Bi}$, is defined by the expression analogous to eq 8. The total average degree of binding of MANT-ADP on the DnaC protein, associated as the allosteric hexamer on the DnaB helicase, $\Sigma\theta_{Ai}$, is defined by eq 14, while the total average degree of binding of MANT-ADP on the free DnaC protein, $\Sigma\theta_{Ci}$, is defined by

$$\sum \Theta_{Ci} = \frac{K_C[N]_F}{1+K_C[N]_F}$$

(18)

The observed signal, ΔF_{obs}, is then

$$\Delta F_{obs} = 0.07716 \left(\sum \Theta_{Bi} \right) - 0.02442 \left(\sum \Theta_{Bi} \right)^2 + 0.004355 \left(\sum \Theta_{Bi} \right)^3$$

(19)

and the total MANT-ADP concentration, $[N]_T$, at any titration point, is

$$[N]_T = \left(\sum \Theta_{Bi} \right) [DnaB(hexamer)]_T + \left(\sum \Theta_{Ai} \right) [DnaC(hexamer)] + \left(\sum \Theta_{Ci} \right) [DnaC(monomer)]_F$$

(20)

where $[DnaB(hexamer)]_T$, is the total concentration of the DnaB hexamer in the sample. The quantity $[DnaC(hexamer)]$ is the concentration of the DnaC protein as the allosteric hexamer bound to the DnaB helicase, i.e., equal to $[DnaB(hexamer)]_T$, and $[DnaC(monomer)]$ is the concentration of the free monomeric DnaC protein, i.e., $[DnaC(monomer)] = [DnaC]_T - 6[DnaC (hexamer)]$.

As we pointed out, the system is formidably complex. There are five binding parameters, K, σ, K_C, K_A, and K_{MC}, describing the nucleotide binding to the tertiary complex. However, the situation is simplified by the fact that we know the binding of the nucleotide to the DnaC protein in the tertiary complex with the DnaB helicase engaged in the interactions with NDP and the nucleotide binding to the DnaC in the presence of the same DNA oligomer concentration; i.e., we know that $K_C = 9 \times 10^5$ M^{-1}, $K_A = 0.005$, and $K_{MC} = 7.9 \times 10^5$ M^{-1} (see above). Thus, there are only two remaining parameters, K and σ, that must be determined. The solid lines in Figure 10a are the nonlinear least-squares fits of the experimental isotherms for binding of MANT-ADP to the tertiary DnaB–DnaC–ssDNA complex, with a single set of binding parameters, that provide an intrinsic binding constant K of $(3\pm0.5)\times 10^7$M^{-1} and a σ of 0.35 ± 0.05. The theoretical plots are in excellent agreement with the experimental titration curves. The obtained data indicate that binding of the nucleotide cofactor to the DnaC protein is largely independent of the cofactor binding to the helicase. However, the opposite is not true. The intrinsic affinity of the nucleotide is increased by 1 order of magnitude as compared to that of the DnaB–ssDNA complex in the absence of the DnaC protein. Nevertheless, the negative cooperativity parameters are similar for both complexes (see Discussion).

Binding of MANT-ATP to the DnaC Protein in the Presence of the ssDNA, Engaged in the Binary DnaB–DnaC Complex and in the Tertiary DnaB–DnaC–ssDNA Complex

In the final sets of experiments, we addressed the binding of the ATP analogue MANT-ATP to the DnaC protein, free, in the presence of the ssDNA, engaged in the binary DnaB–DnaC complex, and engaged in the tertiary DnaB–DnaC–ssDNA complex. Fluorescence titrations of the DnaC protein alone and in the presence of two different concentrations of the ssDNA oligomer, dA(pdA)$_{19}$, with MANT-ATP, are shown in Figure 11a. The behavior of the system is different from the analogous behavior of the ADP analogue (Figure 6). Increasing the nucleic acid concentration does not systematically decrease the observed fluorescence emission of the bound ATP analogue. At lower dA(pdA)$_{19}$ concentrations, the observed fluorescence change is even larger than that obtained in the absence of the nucleic acid and

slightly lower than that determined for the free protein, at the highest nucleic acid concentration applied (Figure 11a). The solid lines in Figure 11a are the nonlinear least-squares fits of the experimental titration curves for the binding of MANT-ATP to the DnaC, free and in the presence of the ssDNA, using the single-site binding model defined by eq 10. The fits provide intrinsic binding constants (K) of $(3\pm0.5) \times 10^5 M^{-1}$ for free DnaC and $(4\pm0.8) \times 10^5$ and $(6 \pm 1.2) \times 10^5 M^{-1}$ for the lower and higher concentrations of the ssDNA 20-mer, respectively. Similar to the case for the ADP analogue, the increase in the nucleic acid concentration increases the intrinsic affinity of MANT-ATP for the nucleotide-binding site of the DnaC protein. However, the effect is much less pronounced. At the highest $dA(pdA)_{19}$ concentration applied, the binding constant increases by a factor of ~1.5, as compared to the ~7-fold increase observed for MANT-ADP (see Discussion).

Fluorescence titrations of the DnaC protein, engaged in the binary DnaB–DnaC complex with MANT-ATP, in buffer T4, containing 2 mM GDP, are shown in Figure 11b. The fluorescence titration of the free DnaC protein, at the same replication factor concentration with MANT-ATP, is also included in Figure 11b. The fluorescence increase accompanying the binding of the nucleotide analogue to the DnaC protein in the complex with the helicase is dramatically larger, ~5-fold, than that observed for the free protein, indicating a very different effect of the interactions with the helicase on the nucleotide-binding site of the replication factor, as compared to the analogous complex with the ADP analogue (see above). Nevertheless, the apparent cooperativity is evident in the sigmoidal initial part of the titration curve, albeit less pronounced than in the case of MANT-ADP. The solid line in Figure 11b is the nonlinear least-squares fit of the experimental titration curve according to the allosteric MWC model, using eqs 13–15 with two fitting parameters, K_{MC} and K_A. The fit provides an intrinsic binding constant K_{MC} of $(2.4 \pm 0.5) \times 10^5 M^{-1}$ and an allosteric constant K_A of 0.6 ± 0.03. Thus, unlike MANT-ADP, the presence of the helicase has little effect on the intrinsic binding constant of the ATP analogue and the DnaC protein. Also, the allosteric constant is ~6-fold higher than that determined for the ADP analogue.

An analogous fluorescence titration of the DnaC protein in the tertiary DnaC–DnaB–$dA(pdA)_{19}$ complex, with MANT-ATP, is shown in Figure 11c. The fluorescence titration of the binary DnaB–DnaC complex is also included in Figure 11c. In contrast to the ADP analogue, the presence of the nucleic acid decreases 2-fold the fluorescence emission of the ATP analogue, accompanying the binding of the cofactor to the DnaC protein in the tertiary as compared to the binary DnaB–DnaC complex. These data indicate that in the presence of the nucleic acid, the helicase affects the structure of the nucleotide-binding site of the DnaC protein, but the effect remains different from the one observed for the ADP analogue (Figure 9b). The solid line in Figure 11c is the nonlinear least-squares fit of the experimental titration curve according to the allosteric model, using eqs 13–15 with two fitting parameters, K_{MC} and K_A, which provides an intrinsic binding constant K_{MC} of $(2.4 \pm 0.5) \times 10^5 M^{-1}$ and an allosteric constant K_A of 0.5 ± 0.03. Contrary to the ADP analogue, neither the intrinsic binding constant nor the apparent cooperativity in the binding of MANT-ATP to the DnaC protein, in the complex with the DnaB helicase, is, within experimental accuracy, affected by the presence of the bound ssDNA (see Discussion).

DISCUSSION

At Saturation, the DnaB Hexamer Associated with the ssDNA Binds Six Nucleotide Cofactors

The maximum stoichiometry or the maximum number of nucleotide cofactor molecules that can associate with the oligomeric helicase is an essential parameter that indicates how many active sites of the enzyme can engage in its physiological functions (48,49,56). In other words, the knowledge of the maximum stoichiometry is of paramount importance in

determining the mechanism of the enzyme. The maximum stoichiometries of the DnaB–nucleotide cofactor complex for the helicase associated with the ssDNA, in the binary DnaB–DnaC complex and in the tertiary DnaB–DnaC–ssDNA complex, as compared to the free enzyme, have been determined in direct binding experiments with the fluorescent nucleotide analogue MANT-GDP. Competition studies with unmodified nucleotides have shown that the analogue strictly binds to the nucleotide-binding sites of the helicase (25). At saturation, the free DnaB hexamer binds six MANT-GDP molecules in a binding process characterized by negative cooperative interactions (Figure 1a,b) (19,25). In the case of the DnaB–ssDNA complex, we could determine the average degree of binding, $\Sigma\theta_i$, of the nucleotide analogue up to ~5 cofactor molecules per DnaB hexamer. Short extrapolation to the maximum value of the observed fluorescence quenching, ΔF_{max}, provides the maximum $\Sigma\theta_i$ value of 6 ± 0.3 (Figure 3b). Thus, we have established that, at saturation, the DnaB hexamer, engaged in the complex with the ssDNA, can bind six molecules of nucleotide cofactors, similar to the free enzyme (19,25).

Nevertheless, the bound ssDNA affects the relative protein fluorescence quenching accompanying binding of MANT-GDP to the helicase as compared to the free enzyme. The effect is particularly pronounced in the high-affinity binding phase, i.e., the phase in which the first three nucleotide molecules associate with the enzyme (Figures 1b and 3b). It is reflected in a lower value of the first parameter in the empirical function $\Delta F_{obs}(\Sigma\theta_i)$ ($a_1 \approx 0.167$), while for the free enzyme, $a_1 \approx 0.187$. Notice that the nucleic acid is bound in the cross channel of the hexamer to a single subunit of the enzyme (17). Because the nucleotide-binding sites are initially independent and identical, the first nucleotide cofactor can bind to any of the six subunits of the enzyme. Moreover, the nucleotide-binding sites are located on the outside surface of the protein (19, 24). Thus, the ssDNA, bound to a single subunit inside the cross channel, must affect the structure of all six nucleotide-binding sites of the hexamer, indicating an allosteric effect of the nucleic acid extends not only through a single subunit but also through the entire hexamer. Moreover, the effect is particularly prominent for the first two to three nucleotide molecules bound, strongly suggesting specific interplay between the nucleotides associated in the high-affinity binding phase and the ssDNA (Figures 1b and 3b). These results corroborate the recent findings for the analogous, plasmid RSF1010 RepA hexameric helicase, which indicate that binding of the first two nucleotides, i.e., the nucleotides that associate in the high-affinity phase, predominantly controls the interactions of the enzyme with the ssDNA and the accompanying conformational transitions of the helicase (31).

The ssDNA Dramatically Increases the Intrinsic Affinity of the ATP Nonhydrolyzable Analogue AMP-PNP for the Nucleotide-Binding Site of the DnaB Hexamer, while the Nucleic Acid Has Little Effect on the Intrinsic Affinities of the GDP or ADP Analogues

Recall that only in the presence of the ATP or NTP nonhydrolyzable analogues, but not ADP or NDP, does the affinity of the DnaB helicase for the ssDNA increase by ~3–4 orders of magnitude, as compared to the affinity in the absence of the cofactor (12–14,19). This thermodynamic linkage between nucleic acid binding and the type of cofactor is clearly seen in the effect of the ssDNA on the binding of the AMP-PNP, ADP, and GDP analogues to the enzyme in the stationary complex, i.e., in the absence of NTP hydrolysis. The intrinsic affinity of AMP-PNP is increased by ~3–4 orders of magnitude, while the presence of the bound ssDNA 20-mer only slightly affects the intrinsic affinity of MANT-GDP or MANT-ADP for the DnaB helicase, making the affinity difference between the ATP and NDP analogue as large as ~3–4 orders of magnitude and possibly larger than that. However, as we described in the companion paper (DOI 10.1021/bi9000529), the presence of the ssDNA only modestly increases the intrinsic affinity of ATP, which enters the hydrolysis, as compared to the free enzyme. Nevertheless, to perform efficient free energy transduction,

the NTP affinity must be much larger than the NDP affinity [companion paper (DOI 10.1021/bi9000529)], and at least comparable to the affinity difference observed between their stationary complexes. Thus, these data indicate that the stationary complexes, which do not enter the hydrolysis reaction, reflect allosteric interactions between the DNA- and NTP-binding site prior to the hydrolysis step and subsequent to product release. In other words, hydrolyzable NTPs enter reaction pathways, after initial recognition steps, different from those observed for the stationary complexes [companion paper (DOI 10.1021/bi9000529)]. The presence of the bound ssDNA does not significantly affect the negative cooperativities of the analogue binding. Thus, the separation of the high- and low-affinity phases in the nucleotide binding process remains in the DnaB–ssDNA complex (see below).

In the Binary DnaB–DnaC Complex, the DnaB Helicase Binds Six Nucleotide Cofactors. However, the DnaC Protein Diminishes the Intrinsic Affinity and Increases the Negative Cooperativity in the Binding of the Cofactor to the DnaB Helicase

The maximum stoichiometry of the binding of the nucleotide to the DnaB helicase in the binary DnaB–DnaC complex has been addressed using the sedimentation velocity method (Figure 2b). These data have unequivocally established that, in the presence of the DnaC protein associated with the helicase, six nucleotide molecules bind to the enzyme (Figure 2b). Thus, in the binary complex, all six nucleotide-binding sites can still engage in interactions with the cofactors. Striking features of the fluorescence titration of the DnaB–DnaC complex with MANT-GDP in Figure 2a are the diminished intrinsic affinity and the considerably increased negative cooperativity, as compared to those of the free helicase, with an intrinsic binding constant K of $\approx 4 \times 10^5 M^{-1}$ and a σ of ≈ 0.08, as compared to a K of $\approx 1 \times 10^6$ M^{-1} and a σ of ≈ 0.27, determined for the free enzyme. Nevertheless, the excellent agreement with the total average degree of binding, predicted with the same empirical function, $\Delta F_{obs}(\Sigma\theta_i)$, that was used for the free enzyme and obtained using the sedimentation velocity method, indicates that the bound DnaC protein does not affect the structure of the nucleotide-binding sites of the helicase as does the ssDNA bound in the cross channel (see above).

There are two important aspects of these data. First, the DnaC protein is not a "neutral attachment gear", which allows the helicase to recognize the replisome and/or preprimosome, but the protein significantly affects the helicase–nucleotide interactions (8,9). This is also clearly seen in the simultaneous binding of the cofactor to both protein components of the tertiary complex, where the intrinsic affinity of the nucleotide for the helicase is significantly increased (Figure 10a). The effect is not limited to a single subunit but is extended through the entire hexamer, as indicated by the strong increase in the negative cooperativity in the cofactor binding to the helicase. Second, by increasing the negative cooperativity, the bound DnaC protein effectively increases the separation between the high- and low-affinity binding phases in the nucleotide binding to the enzyme (Figure 2a). Recall that the binary DnaB–DnaC complex is the entity that recognizes the replisome and/or preprimosome (1,4,8,9,21). Thus, these results indicate that in the recognition process, where the helicase must associate with the ssDNA, the binary complex is preferentially in a state in which the helicase is mostly associated with only one to three nucleotide cofactors. As pointed out above, binding of the first two nucleotides in the high-affinity phase predominantly controls interactions of the analogous RepA helicase with the ssDNA, through global conformational changes of the enzyme (31). Binding of the DnaC protein reinforces the state of the DnaB hexamer, in which the hexameric helicase achieves the highest conformational flexibility in the recognition process vis-à-vis the nucleic acid.

In the Tertiary DnaB–DnaC–ssDNA Complex, the Effect of the DnaC Protein on the Helicase–Nucleotide Interactions Is Attenuated by the Nucleic Acid

Similar to that of the binary complex discussed above, the maximum stoichiometry of the nucleotide binding to the DnaB helicase in the tertiary DnaB–DnaC–ssDNA complex has been addressed using the sedimentation velocity method, which unambiguously establishes that six nucleotide molecules bind to the helicase (Figure 5b). Thus, the data obtained in this work show that the DnaB helicase never looses the ability to engage all six nucleotide-binding sites in interactions with the cofactor, in all examined complexes (19). However, the presence of the nucleic acid strongly increases both the intrinsic affinity and cooperativity parameter for the binding of the cofactor to the helicase in the tertiary complex, with an intrinsic binding constant K of $\approx 2.1 \times 10^6 \, M^{-1}$ and a σ of ≈ 0.5, as compared to the helicase in the binary complex, characterized by a K of $\approx 4 \times 10^5 M^{-1}$ and a σ of ≈ 0.08 (Figure 5a). Thus, the nucleic acid attenuates the effect of the DnaC protein alone and diminishes the separation between the high- and low-affinity phases in nucleotide binding to the enzyme (see above). As discussed above, this would lead to a diminished conformational flexibility of the helicase in the ssDNA recognition process and in the complex with the ssDNA in general.

However, the tertiary DnaB–DnaC–ssDNA complex is a past-ssDNA-recognition complex with different physiological functions (1,4,8,9,21). When bound to the nucleic acid, the helicase performs mechanical translocation on the nucleic acid lattice and/or dsDNA unwinding (35,36,39,44). The DnaB helicase can also act as a molecular pump by moving the DNA through the cross channel of the ringlike hexameric structure (57,58). Recall that we have examined the behavior of the DnaB–DnaC–ssDNA complex with six DnaC molecules bound (see above). Because the conformational flexibility of the enzyme is crucial for translocation and unwinding activities, as indicated by the data on the analogous RepA hexamer and controlled by the first two to three nucleotides bound, the data indicate that the presence of the six bound DnaC molecules in the tertiary complex would inhibit the translocation and unwinding activities (31). In other words, these results suggest that to achieve optimal translocation and unwinding capacity, the helicase must release at least some of the six DnaC molecules from the tertiary complex. This conclusion strongly corroborates biochemical data, indicating that the excess of the DnaC protein inhibits the elongation stage of DNA replication (59,60). Notice that such inhibition can be observed only if fewer than six DnaC molecules are bound to the enzyme.

On the other hand, the molecular pump activity could be reinforced by the presence of the DnaC protein, as the helicase requires less conformational flexibility, as indicated by the data on the RepA hexamer and the efficient participation of all six NTPase sites engaged in the complex with the cofactor (31). Strongly increased intrinsic affinity and decreased negative cooperativity can accomplish that. Also notice that the maximum quenching of the protein fluorescence accompanying the nucleotide binding to the tertiary complex is significantly lower ($\Delta F_{max} \approx 0.35$) than that ($\Delta F_{max} \approx 0.63$) determined for the free enzyme, associated with the ssDNA, or in the binary complex (Figure 5a). Such a considerable structural difference also indicates that the structure of the examined tertiary complex is very different from all complexes in which the helicase does preserve its conformational flexibility necessary for translocation, dsDNA unwinding, and ssDNA recognition discussed above (31).

The DnaC Protein Retains Its Nucleotide Binding Ability in the Binary DnaB–DnaC and Tertiary DnaB–DnaC–ssDNA Complexes

Quantitative thermodynamic studies have shown that six molecules of the DnaC replication factor, associated with the DnaB helicase, form a hexamer in which the subunits (DnaC

molecules) are linked through the positive cooperative interactions (11). Whether all DnaC molecules, in such an assembled hexamer, retain nucleotide binding ability is not a priori certain. This is particularly true if one considers that the DnaC protein exists in solution in two conformations, prior to nucleotide binding, with only one conformation capable of binding the cofactors (see below) (27,28,55). The sedimentation velocity approach, applied in this work, clearly shows that in the binary DnaB–DnaC and tertiary DnaB–DnaC–ssDNA complexes, each bound DnaC molecule possesses nucleotide binding ability (Figures 8b and 9b). This is true for both ADP and ATP analogues (data not shown). In other words, the functioning of these complexes requires that all bound DnaC molecules be able to bind a cofactor.

The DnaC Protein Controls the DnaB–DnaC Complex through an Allosteric Transition of the Entire DnaC Hexamer Assembled on the Helicase

A remarkable feature of binding of a nucleotide to the DnaC protein, in the complex with the DnaB helicase, is an apparent positive cooperativity characterizing the binding process (Figures 8a and 9a). The cooperativity is particularly pronounced in the tertiary DnaB–DnaC–ssDNA complex. This type of binding process could be described by the simple hexagon model (eqs 6–8). Although the hexagon model cannot be completely ruled out, such a model would ignore the fact that the DnaC protein exists in solution in equilibrium between two conformational states with one of the states not capable of binding the cofactors (27, 28, 55). Moreover, the simple hexagon model does not take into account the fact that the nucleotide induces conformational transitions in the DnaC protein. Hydrodynamic data indicate that in the presence of saturating concentrations of ADP, the DnaC protein assumes a more elongated and rigid global structure, as compared to the free protein or protein saturated with ATP (30). The allosteric MWC model is the simplest extension of the known behavior of the DnaC protein, in terms of the nucleotide binding, to its complex with the DnaB hexamer (26–30).

The value of the allosteric transition constant characterizing the conformational transition between two conformations of the free DnaC protein (K_A) is ≈ 5 (27,28). This is a modest value. Nevertheless, it indicates that the preferred conformation of the replication factor in solution is the state that binds the nucleotide cofactors. In the binary DnaB–DnaC and tertiary DnaB–DnaC–ssDNA complexes, the values of the allosteric constant (K_A), characterizing the ADP analogue binding, are ≈ 0.1 and ≈ 0.005, respectively (Figures 8a and 9a). These values of K_A, which are ~2 and ~3 orders of magnitude smaller, respectively, than the K_A determined for the free protein, indicate that the DnaB helicase preferentially stabilizes the DnaC conformation, which does not bind ADP. This is particularly pronounced in the tertiary complex with the ssDNA. In the context of our discussion of the effect of the DnaC protein on the DnaB helicase in the tertiary complex (see above), it should be noted that the DnaC protein has the highest affinity for the DnaB helicase in the presence of ADP (11). Considerably cooperative binding of the ADP analogue to the DnaC protein in the tertiary complex indicates that a small change in the ADP concentration will induce significant changes in the affinity of the protein for the helicase. Thus, the data strongly suggest that a possible partial release of some of the DnaC protein molecules from the tertiary complex and return of the helicase to the state of an increased conformational flexibility is under the strict control of the binding of the nucleotide to the replication factor, not the helicase.

Figure 12 shows a schematic model of the allosteric transition of the six DnaC protein molecules bound to the DnaB hexamer in the tertiary DnaB–DnaC–ssDNA complex, based on the thermodynamic data described in this work. The DnaB helicase preferentially stabilizes the DnaC protein in the conformation in which the replication factor does not possess nucleotide binding capability (37, 38). The DnaC protein is in a less elongated state,

as indicated by the hydrodynamic data (30). The binary DnaB–DnaC complex and the tertiary DnaB–DnaC–ssDNA complex, with six DnaC molecules assembled as a hexamer on the DnaB protein, also exit in solution in an equilibrium between two conformations of the assembled DnaC hexamer, with only one conformation of the DnaC hexamer capable of binding nucleotide cofactors. Binding of a single nucleotide cofactor to one of the bound DnaC molecules induces the transition of the entire DnaC hexamer into the conformation, which has significant affinity for the nucleotide cofactor. This DnaC conformation also has a more elongated global structure (30).

Allosteric Interactions between the Nucleotide- and Nucleic Acid-Binding Sites of DnaC Depend on the Structure of the Phosphate Group of the Bound Cofactor

Thermodynamic studies of the cofactor binding to the free DnaC protein already indicated significant differences between ADP and ATP binding (26,30). Thus, while the affinity of the ATP analogue increases with an increase in Mg^{2+} concentration, the affinity of the ADP analogue strongly decreases, indicating not only a simple competition but also allosteric interactions between the magnesium and the nucleotide-binding sites on the protein. In turn, these allosteric interactions depend on the phosphate group structure of the cofactor. Hydrodynamic and spectroscopic studies of the DnaC–nucleotide complex clearly showed significant differences in the effect of ADP versus ATP on the protein structure, which include both local nucleotide-binding site structural changes and the global structure of the protein (26,30). Allosteric interactions between the weak nucleic acid-binding site and the nucleotide-binding site of the DnaC protein are clearly observed in the titrations of the protein with the cofactors, in the presence of the ssDNA 20-mer, and these interactions are different for ADP and ATP (Figures 6 and 11). The dramatic differences in the induced changes of the MANT-ADP fluorescence versus MANT-ATP provide strong evidence that the nucleic acid affects the structure of the nucleotide-binding site of the protein, making it much less hydrophobic in the case of ADP (29). We could not examine the DNA effect at the saturation concentration of the nucleic acid, due to the low affinity and the propensity of the system to precipitate. Nevertheless, at the highest concentration of the ssDNA oligomer applied, the intrinsic binding constant of the ADP analogue is increased by almost 1 order of magnitude, while the intrinsic affinity of the ATP analogue increases by a factor of only ~2. Thus, the structure of the DnaC protein, generated by the nucleotide triphosphate binding, is less prone to the effect of the nucleic acid, as compared to the complex containing a nucleotide diphosphate.

The Cooperativity of the Allosteric Transition of the DnaC Hexamer, Assembled on the DnaB Helicase, Depends on the Structure of the Phosphate Group of the Bound Adenosine Nucleotide

The most striking difference between the ADP and ATP analogues is observed in the association of the cofactor with the replication factor in the binary DnaB–DnaC and tertiary DnaB–DnaC–ssDNA complexes. Both cofactors exhibit positive cooperativity in the binding process. However, the similarity ends here. The allosteric constants, K_A, characterizing the binding of ADP to the binary and tertiary complex are lower by factors of ~5 and ~100, respectively, than the analogous parameters determined for the ATP analogue. Such a large difference may be rather surprising because K_A characterizes an intrinsic transition of the assembled DnaC hexamer on the DnaB helicase and is not directly related to the intrinsic, nucleotide binding process. On the other hand, K_A will depend on the final structure of the DnaC protein, bound to the DnaB helicase, generated by the specific cofactor. In light of the findings of different structures of the DnaC protein generated by ADP and ATP binding, the large difference between the corresponding values of K_A should not be that surprising. In other words, the differences in K_A values between ADP and ATP

analogues reflect the presence of different, final conformational states of the DnaC protein, when associated with the ADP or ATP analogue (30).

The data and analyses described in this work indicate that the DnaC protein affects the DnaB–DnaC complex on two different levels, strictly related to the functional activities of the complex. The first level concerns the effect on the DnaB helicase and its translocation and dsDNA unwinding activities. The second level is the control through the changes in the DnaC protein itself, which includes global structural changes of the assembled DnaC protein hexamer on the helicase. Recall that the DnaC protein is absolutely necessary for the helicase to recognize the replisome and/or the preprimosome (1,8,9). The conformational differences between various DnaB–DnaC complexes, resulting from the structural changes in the bound DnaC protein, controlled by the nucleotide cofactor binding, are more than certain to be involved in these extremely specific recognition processes. Our laboratory is currently examining these aspects of the DnaB–DnaC complex activities.

Acknowledgments

References

1. Kornberg, A.; Baker, TA. DNA Replication. Freeman; San Francisco: 1992.

2. Kim S, Dallman G, McHenry CS, Marians KJ. Coupling of a Replicative Polymerase and Helicase: A τ-DnaB Interactions Mediates Rapid Replication Fork Movement. Cell. 1996; 84:643–650. [PubMed: 8598050]

3. Heller RC, Marians KJ. Non-Replicative Helicases at the Replication Fork. DNA Repair. 2007; 6:945–952. [PubMed: 17382604]

4. Marszalek J, Kaguni JM. DnaA protein directs the binding of the DnaB protein in initiation of DNA replication. J Biol Chem. 2001; 276:44919–44925. [PubMed: 11551962]

5. Roman LJ, Eggleston AK, Kowalczykowski SC. Processivity of the DNA helicase activity of the *Escherichia coli* RecBCD enzyme. J Biol Chem. 1992; 267:4207–4214. [PubMed: 1310990]

6. North SH, Nakai H. Host Factors That Promote Transpososome Disassembly and the PriA-PriC Pathway For Restart Primosome Assembly. Mol Microbiol. 2005; 56:1601–1616. [PubMed: 15916609]

7. Baker T, Funnel BE, Kornberg A. Helicase Action of dnaB Protein during Replication from *Escherichia coli* Chromosomal Origin *in Vitro*. J Biol Chem. 1987; 262:6877–6885. [PubMed: 3032979]

8. Wahle E, Lasken RS, Kornberg A. The dnaB-dnaC Replication Protein Complex of *Escherichia coli*. I Formation and Properties. J Biol Chem. 1989; 264:2463–2468. [PubMed: 2536712]

9. Wahle E, Lasken RS, Kornberg A. The dnaB-dnaC Replication Protein Complex of *Escherichia coli* II. Role of the Complex in Mobilizing dnaB Functions. J Biol Chem. 1989; 264:2469–2475. [PubMed: 2536713]

10. LeBowitz JH, McMacken R. The *Escherichia coli* dnaB Replication Protein Is a DNA Helicase. J Biol Chem. 1986; 261:4738–4748. [PubMed: 3007474]

11. Galletto R, Jezewska MJ, Bujalowski W. Interactions of the *Escherichia coli* DnaB Helicase Hexamer with the Replication Factor the DnaC Protein. Effect of Nucleotide Cofactors and the ssDNA on Protein-Protein Interactions and the Topology of the Complex. J Mol Biol. 2003; 329:441–465. [PubMed: 12767828]

12. Bujalowski W, Jezewska MJ. Interactions of *Escherichia coli* Primary Replicative Helicase DnaB Protein with Single-Stranded DNA. The Nucleic Acid Does Not Wrap Around the Protein Hexamer. Biochemistry. 1995; 34:8513–8519. [PubMed: 7612593]

13. Jezewska MJ, Kim US, Bujalowski W. Binding of *Escherichia coli* Primary Replicative Helicase DnaB Protein to Single-Stranded DNA. Long-Range Allosteric Conformational Changes within the Protein Hexamer. Biochemistry. 1996; 35:2129–2145. [PubMed: 8652555]

14. Jezewska MJ, Bujalowski W. A General Method of Analysis of Ligand Binding to Competing Macromolecules Using the Spectroscopic Signal Originating from a Reference Macromolecule. Application to *Escherichia coli* Replicative Helicase DnaB Protein-Nucleic Acid Interactions. Biochemistry. 1996; 35:2117–2128. [PubMed: 8652554]

15. Jezewska MJ, Rajendran S, Bujalowski W. Strand Specificity in the Interactions of *Escherichia coli* Primary Replicative Helicase DnaB Protein with Replication Fork. Biochemistry. 1997; 36:10320–10326. [PubMed: 9254631]

16. Jezewska MJ, Rajendran S, Bujalowski W. Functional and Structural Heterogeneity of the DNA Binding of the *E. coli* Primary Replicative Helicase DnaB protein. J Biol Chem. 1998; 273:9058–9069. [PubMed: 9535894]

17. Jezewska MJ, Rajendran S, Bujalowska D, Bujalowski W. Does ssDNA Pass Through the Inner Channel of the Protein Hexamer in the Complex with the *E. coli* DnaB Helicase? Fluorescence Energy Transfer Studies. J Biol Chem. 1998; 273:10515–10529. [PubMed: 9553111]

18. San Martin C, Radermacher M, Wolpensinger B, Miles CS, Dixon NE, Caraza JM. Three-Dimensional Reconstructions From Cryoelectron Microscopy Images an Intimate Complex Between Helicase DnaB and Its Loading Partner DnaC. Structure. 2005; 6:501–509. [PubMed: 9562559]

19. Bujalowski W, Klonowska MM, Jezewska MJ. Oligomeric Structure of *Escherichia coli* Primary Replicative Helicase DnaB Protein. J Biol Chem. 1994; 269:31350–31358. [PubMed: 7989299]

20. Jezewska MJ, Bujalowski W. Global Conformational Transitions in *E. coli* Primary Replicative DnaB Protein Induced by ATP, ADP and Single-Stranded DNA Binding. J Biol Chem. 1996; 271:4261–4265. [PubMed: 8626772]

21. Arai K, Kornberg A. Mechanism of dnaB protein action. Allosteric role of ATP in the alteration of DNA structure by dnaB protein in priming replication. J Biol Chem. 1981; 256:5260–5266. [PubMed: 6262326]

22. Bujalowski W, Jezewska MJ. Kinetic Mechanism of Nucleotide Cofactor Binding to *Escherichia coli* Replicative Helicase DnaB Protein. Stopped-Flow Kinetic Studies Using Fluorescent, Ribose-, and Base-Modified Nucleotide Analog. Biochemistry. 2000; 39:2106–2122. [PubMed: 10684661]

23. Bujalowski W, Klonowska MM. Negative Cooperativity in the Binding of Nucleotides to *Escherichia coli* Replicative Helicase DnaB Protein. Interactions with Fluorescent Nucleotide Analogs. Biochemistry. 1993; 32:5888–5900. [PubMed: 8504109]

24. Bujalowski W, Klonowska MM. Close Proximity of Tryptophan Residues and ATP-binding Site in *Escherichia coli* Primary Replicative Helicase DnaB Protein. Molecular Topography of the Enzyme. J Biol Chem. 1994; 269:31359–31371. [PubMed: 7989300]

25. Jezewska MJ, Kim US, Bujalowski W. Interactions of *Escherichia coli* Primary Replicative Helicase DnaB Protein with Nucleotide Cofactors. Biophys J. 1996; 71:2075–2086. [PubMed: 8889182]

26. Galletto R, Rajendran S, Bujalowski W. Interactions of Nucleotide Cofactors with the *Escherichia coli* Replication Factor DnaC Protein. Biochemistry. 2000; 39:12959–12969. [PubMed: 11041861]

27. Galletto R, Bujalowski W. The *E. coli* Replication Factor DnaC Protein Exists in Two Conformations with Different Nucleotide Binding Capabilities. I Determination of the Binding Mechanism Using ATP and ADP Fluorescent Analogues. Biochemistry. 2002; 41:8907–8920. [PubMed: 12102633]

28. Galletto R, Bujalowski W. Kinetics of the *E. coli* Replication Factor DnaC Protein–Nucleotide Interactions. II Fluorescence Anisotropy and Transient, Dynamic Quenching Stopped-Flow Studies of the Reaction Intermediates. Biochemistry. 2002; 41:8921–8934. [PubMed: 12102634]

29. Galletto R, Jezewska MJ, Maillard R, Bujalowski W. The Nucleotide-Binding Site of the *Escherichia coli* DnaC Protein. Cell Biochem Biophys. 2005; 43:331–353. [PubMed: 16244362]

30. Galletto R, Maillard R, Jezewska MJ, Bujalowski W. Global Conformation of the *Escherichia coli* Replication Factor DnaC Protein in Absence and Presence of Nucleotide Cofactors. Biochemistry. 2004; 43:10988–11001. [PubMed: 15323558]

31. Marcinowicz A, Jezewska MJ, Bujalowski W. Multiple Global Conformational States of the Hexameric RepA Helicase of Plasmid RSF1010 With Different ssDNA-Binding Capabilities Are

Induced By Different Numbers of Bound Nucleotides. Analytical Ultracentrifugation and Dynamic Light Scattering Studies. J Mol Biol. 2008; 375:386–408. [PubMed: 18022636]

32. Rajendran S, Jezewska MJ, Bujalowski W. Multiplestep Kinetic Mechanism of DNA-independent ATP Binding and Hydrolysis by *Escherichia coli* Replicative Helicase DnaB Protein: Quantitative Analysis Using the Rapid Quench-Flow Method. J Mol Biol. 2000; 303:773–795. [PubMed: 11061975]

33. Kobori JA, Kornberg A. The *Escherichia coli dnaC* Gene Product. II Purification, Physical Properties, and Role in Replication. J Biol Chem. 1982; 257:13763–13769. [PubMed: 6292204]

34. Kobori JA, Kornberg A. The *Escherichia coli dnaC* Gene Product, III. Properties of the dnaB-dnaC Protein Complex. J Biol Chem. 1982; 257:13770–13775. [PubMed: 6292205]

35. Galletto R, Jezewska MJ, Bujalowski W. Unzipping Mechanism of the Double-Stranded DNA Unwinding by a Hexameric Helicase. Quantitative Analysis of the Rate of the dsDNA Unwinding, Processivity and Kinetic Step-Size of the *Escherichia coli* DnaB Helicase Using Rapid Quench-Flow Method. J Mol Biol. 2004; 343:83–99. [PubMed: 15381422]

36. Galletto R, Jezewska MJ, Bujalowski W. Unzipping Mechanism of the Double-Stranded DNA Unwinding by a Hexameric Helicase. The Effect of the 3′ Arm and the Stability of the dsDNA on the Unwinding Activity of the *Escherichia coli* DnaB Helicase. J Mol Biol. 2004; 343:101–114. [PubMed: 15381423]

37. Dong F, Gogol EP, von Hippel PH. The Phage T4-coded DNA Replication Helicase (gp41) Forms a Hexamer upon Activation by Nucleoside Triphosphate. J Biol Chem. 1995; 270:7462–7473. [PubMed: 7706292]

38. Hacker KJ, Johnson KA. A Hexameric Helicase Encircles One DNA Strand and Excludes the Other during DNA Unwinding. Biochemistry. 1997; 36:14080–14087. [PubMed: 9369480]

39. Ali JA, Lohman TM. Kinetic Measurement of the Step Size of DNA Unwinding by *Escherichia coli* UvrD Helicase. Science. 1997; 275:377–3380. [PubMed: 8994032]

40. Lucius AL, Vindigni A, Gregorian R, Ali JA, Taylor AF, Smith GR, Lohman TM. DNA Unwinding Step-Size of the *E. coli* RecBCD Helicase Determined from Single- Turnover Chemical Quenched-Flow Kinetics. J Mol Biol. 2002; 324:409–428. [PubMed: 12445778]

41. Nanduri B, Byrd AK, Eoff RL, Tackett AJ, Raney KD. Pre-steady state DNA unwinding by bacteriophage T4 Dda helicase reveals a monomeric molecular motor. Proc Natl Acad Sci USA. 2002; 99:14722–14727. [PubMed: 12411580]

42. Jankowsky E, Gross CH, Shuman S, Pyle AM. The DexH protein NPH-II is a processive and directional motor for unwinding RNA. Nature. 2002; 403:447–451. [PubMed: 10667799]

43. Young MC, Kuhl SB, von Hippel PH. Kinetic Theory of ATP-driven Translocases on One-dimensional Polymer Lattices. J Mol Biol. 1994; 235:1436–1446. [PubMed: 8107084]

44. Lohman TM, Bjornson KP. Mechanisms of Helicase-Catalyzed DNA Unwinding. Annu Rev Biochem. 1996; 65:169–214. [PubMed: 8811178]

45. Huang SG, Weisshart K, Fanning E. Characterization of the Nucleotide Binding Properties of SV40 T Antigen Using Fluorescent 3′(2′)-O-(2,4,6-Trinitrophenyl)adenine Nucleotide Analogs. Biochemistry. 1998; 37:15336–15344. [PubMed: 9799494]

46. Bujalowski W, Klonowska MM. Structural Characteristics of the Nucleotide Binding Site of *E. coli* Primary Replicative Helicase DnaB Protein. Studies with Ribose and Base-Modified Fluorescent Nucleotide Analogs. Biochemistry. 1994; 33:4682–4694. [PubMed: 8161526]

47. Bujalowski, W.; Jezewska, MJ. Spectrophotometry & Spectrofluorimetry. In: Gore, MG., editor. A Practical Approach. Oxford University Press; New York: 2000. p. 141-165.

48. Bujalowski W. Thermodynamic and Kinetic Methods of Analyses of Protein–Nucleic Acid Interactions. From Simpler to More Complex Systems. Chem Rev. 2006; 106:556–606. [PubMed: 16464018]

49. Lohman TM, Bujalowski W. Thermodynamic Methods for the Model-Independent Determination of Equilibrium Binding Isotherms for Protein-DNA Interactions, Using Spectroscopic Approaches to Monitor the Binding. Methods Enzymol. 1991; 208:258–290. [PubMed: 1779838]

50. Jezewska MJ, Lucius AL, Bujalowski W. Binding of Six Nucleotide Cofactors to the Hexameric Helicase RepA Protein of Plasmid RSF1010. I. Direct Evidence of Cooperative Interactions

Between the Nucleotide-Binding Sites of a Hexameric Helicase. Biochemistry. 2005; 44:3865–3876. [PubMed: 15751962]

51. Jezewska MJ, Lucius AL, Bujalowski W. Binding of Six Nucleotide Cofactors to the Hexameric Helicase RepA Protein of Plasmid RSF1010. II Base Specificity, Nucleotide Structure, Magnesium, and Salt Effect on the Cooperative Binding of the Cofactors. Biochemistry. 2005; 44:3877–3890. [PubMed: 15751963]

52. Lucius AL, Jezewska MJ, Bujalowski W. The *Escherichia coli* PriA Helicase Has Two Nucleotide-Binding Sites Differing in Their Affinities for Nucleotide Cofactors. I Intrinsic Affinities, Cooperativities, and Base Specificity of Nucleotide Cofactor Binding. Biochemistry. 2006; 45:7202–7216. [PubMed: 16752911]

53. Jezewska MJ, Bujalowski PJ, Bujalowski W. Interactions of the DNA Polymerase X of African Swine Fever Virus With Double-Stranded DNA. Functional Structure of the Complex. J Mol Biol. 2007; 373:75–95. [PubMed: 17765921]

54. Davey MJ, Fang L, McInerney P, Georgescu RE, O'Donnell M. The DnaC helicase loader is a dual ATP/ADP switch protein. EMBO J. 2002; 21:3148–3159. [PubMed: 12065427]

55. Galletto R, Jezewska MJ, Bujalowski W. Kinetics of Allosteric Conformational Transition of a Macromolecule Prior to Ligand Binding. Analysis of Stopped-Flow Kinetic Experiments. Cell Biochem Biophys. 2005; 42:121–144. [PubMed: 15858229]

56. Monod J, Wyman J, Changeux JP. On the Nature of Allosteric Transition: A Plausible Model. J Mol Biol. 1965; 12:918–923. [PubMed: 4285628]

57. Kaplan DL, O'Donnell M. DnaB drives DNA branch migration and dislodges proteins while encircling two DNA strands. Mol Cell. 2002; 10:647–657. [PubMed: 12408831]

58. West SC. DNA helicases: New breeds of translocating motors and molecular pumps. Cell. 1996; 86:177–180. [PubMed: 8706121]

59. Allen GC Jr, Kornberg A. Fine Balance in the Regulation of DnaB Helicase by DnaC Protein in Replication in *Escherichia coli*. J Biol Chem. 1991; 266:22096–22101. [PubMed: 1657989]

60. Allen GC Jr, Dixon NE, Kornberg A. Strand Switching of a Replicative DNA Helicase Promoted by the *E. coli* Primosome. Cell. 1993; 74:713–722. [PubMed: 8395352]
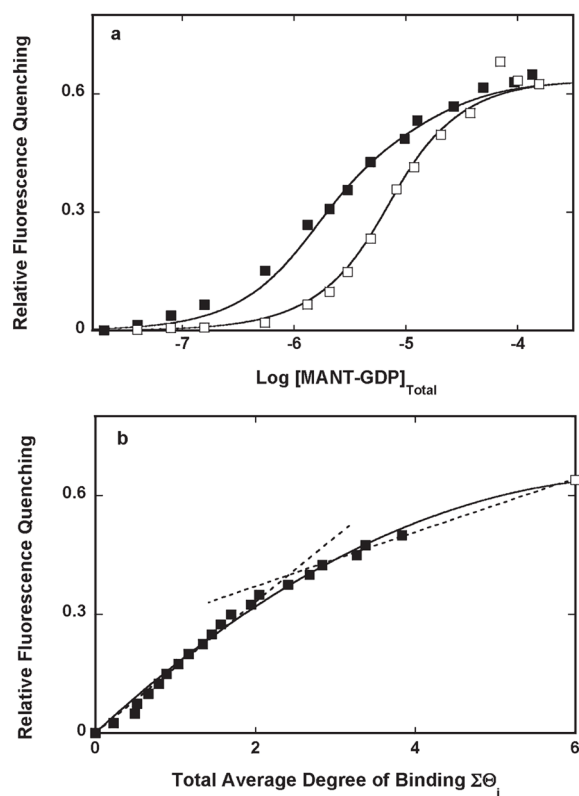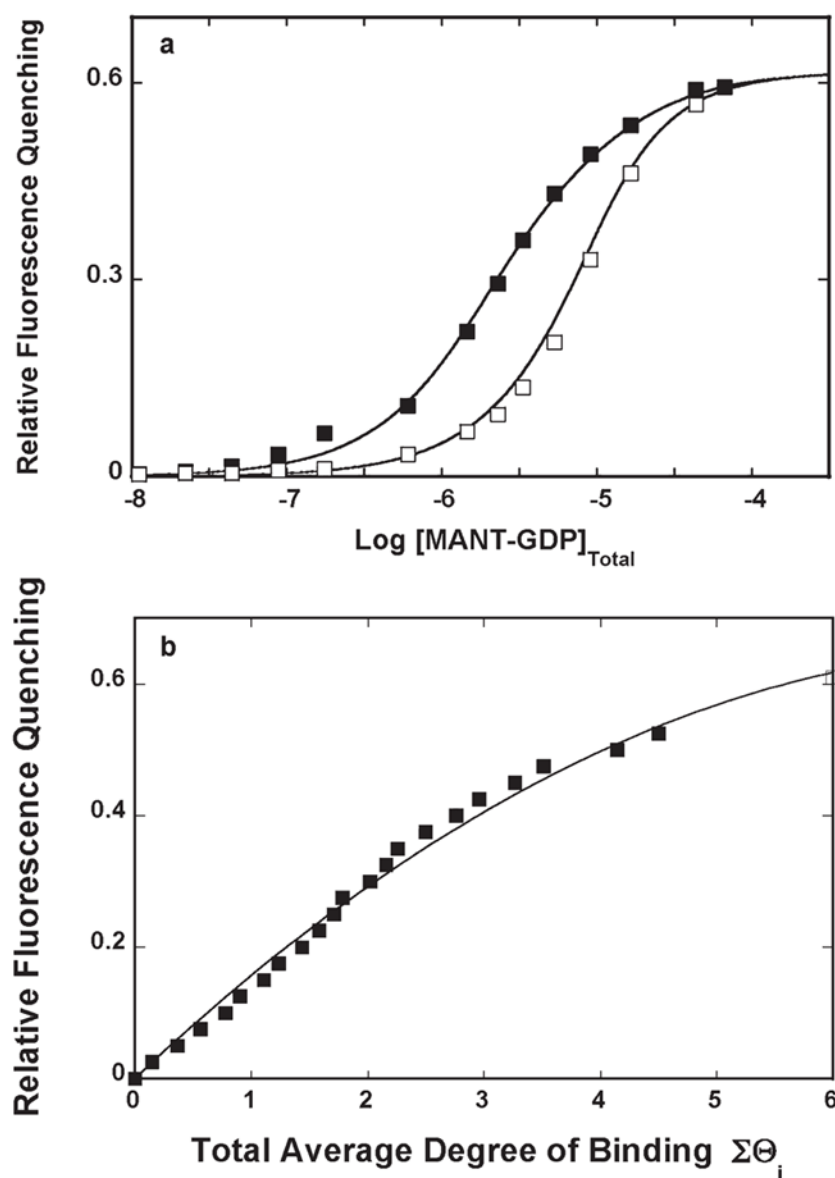
Figure 1.
(a) Fluorescence titration of the DnaB helicase with MANT-GDP in buffer T4 at two different DnaB helicase concentrations: (■) 6×10^{-7} M and (□) 3×10^{-6} M (hexamer). The solid lines are nonlinear least-squares fits of the titration curves, according to the hexagon model (eqs 5–8) using a single set of binding parameters with an intrinsic binding constant K of 1×10^{6} M^{-1} and cooperativity parameter σ of 0.27. The relative fluorescence change, ΔF_{obs}, is defined by the empirical function of the total average degree of binding ,$\Sigma\theta_i$, by eq 8. (b) Dependence of the relative fluorescence increase, ΔF_{obs}, upon the total average degree of binding of MANT-GDP on the DnaB hexamer (■). The values of $\Sigma\theta_i$ have been determined using the quantitative method described in Materials and Methods. The solid line is the nonlinear least-squares fit, using the empirical function, defined by eq 8. The dashed lines mark the slopes of the two binding phases of the ΔF_{obs} dependence upon $\Sigma\theta_i$. The maximum value of the relative fluorescence increase, ΔF_{max}, was 0.63 (□).
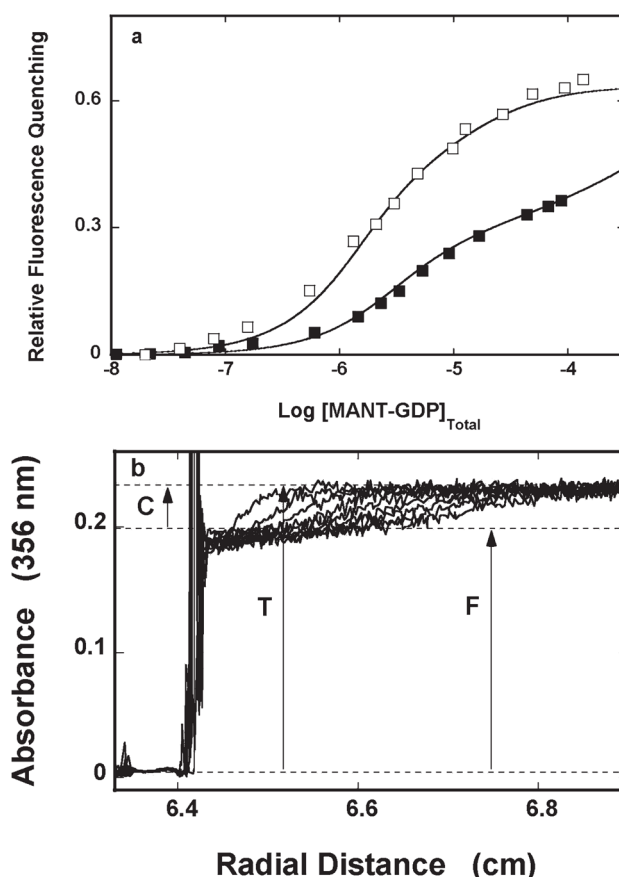
Figure 2.
(a) Fluorescence titration of the DnaB helicase, engaged in the DnaB–DnaC complex, with MANT-GDP in buffer T4 (■). The concentrations of the DnaB and DnaC proteins were 5×10^{-7} M (hexamer) and 5×10^{-6} M, respectively. The solid line is a nonlinear least-squares fit of the titration curve, according to the hexagon model (eqs 5–8) using an intrinsic binding constant K of $4 \times 10^5 M^{-1}$ and a cooperativity parameter σ of 0.08, and the empirical function defined by eq 8. (b) Sedimentation velocity absorption profiles, recorded at 356 nm, of MANT-GDP, in the presence of the DnaB–DnaC complex in buffer T4. The concentrations of the DnaB and DnaC proteins were 1×10^{-6} M (hexamer) and 8×10^{-6} M, respectively. The concentration of the MANT-GDP was 3×10^{-5} M. The scans were conducted at 25000 rpm. The short initial parts of the scans correspond to the buffer–air region above the sample meniscus. The arrows indicate the absorption of the total concentration of MANT-GDP (T), the concentration of the cofactor bound to the DnaB helicase in the DnaB–DnaC complex (C), and the concentration of the free MANT-GDP (F). The horizontal dashed lines indicate the locations of the plateaus corresponding to the zero line, the free MANT-GDP concentration, and the total MANT-GDP concentration (see the text for details).
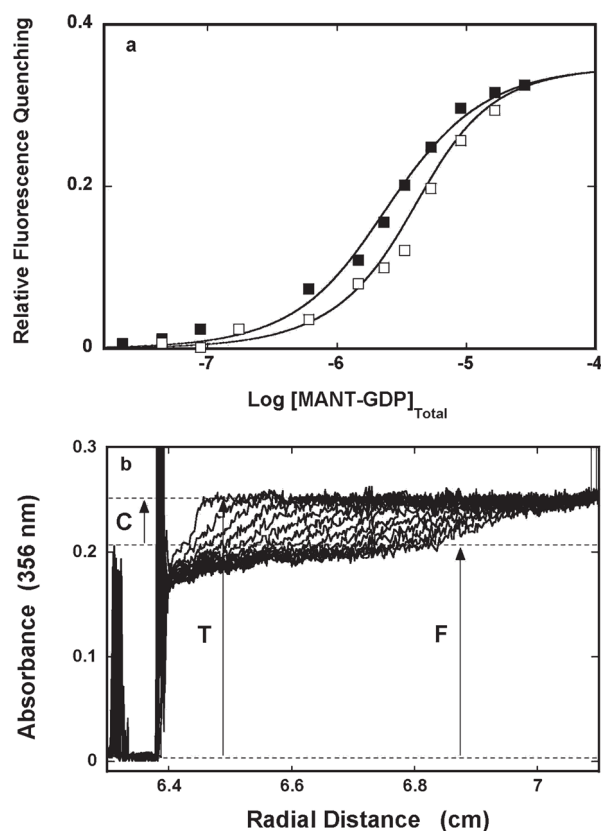
Figure 3.
(a) Fluorescence titration of the DnaB helicase, engaged in the complex with the ssDNA oligomer, $dA(pdA)_{19}$, with MANT-GDP in buffer T4, at two different DnaB concentrations: (■) 6×10^{-7} M and (□) 3×10^{-6} M (hexamer). The concentration of the ssDNA oligomer was 6.5×10^{-5} M. The solid lines are nonlinear least-squares fits of the titration curves, according to the hexagon model (eqs 5–8), using a single set of binding parameters with an intrinsic binding constant K of 9×10^5 M^{-1} and a cooperativity parameter σ of 0.4, and the empirical function defined in the text. (b) Dependence of the relative fluorescence increase, ΔF_{obs}, on the total average degree of binding of MANT-GDP on the DnaB protein, in the complex with the ssDNA oligomer, $dA(pdA)_{19}$, $\Sigma\theta_i$ (■). The values of $\Sigma\theta_i$ have been determined using the quantitative method described in Materials and Methods. The solid line is the nonlinear least-squares fit, using the empirical function defined in the text. The maximum value of the relative fluorescence increase, ΔF_{max}, is 0.61 (□).
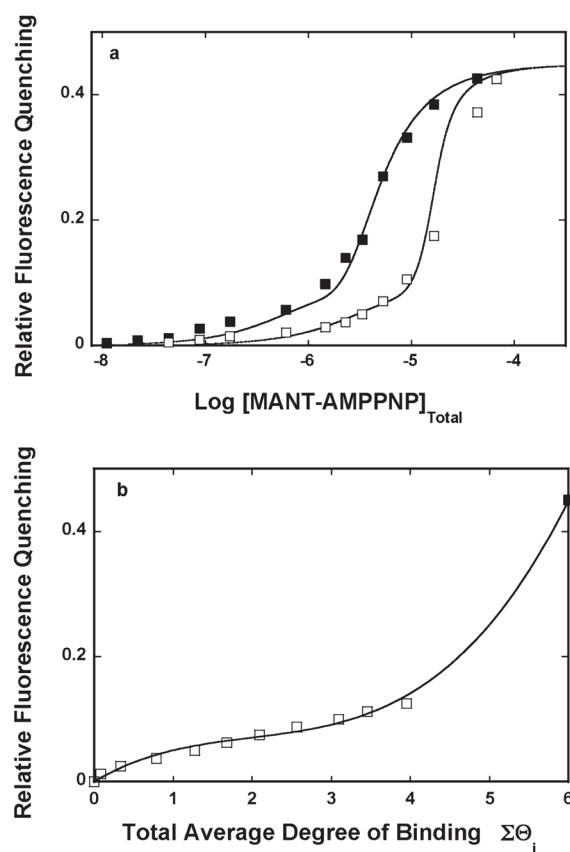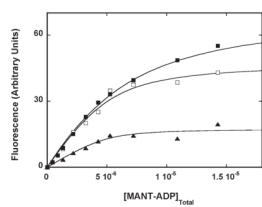
Figure 4.
(a) Fluorescence titrations of the DnaB helicase, engaged in the complex with the ssDNA oligomer, $dA(pdA)_{19}$, with MANT-AMP- PNP in buffer T4, at two different DnaB concentrations: (■) 6×10^{-7} M and (□) 3×10^{-6} M (hexamer). The concentration of the ssDNA oligomer was 6.5×10^{-5} M. The solid lines are nonlinear least-squares fits of the titration curves, according to the hexagon model (eqs 5–8), using a single set of binding parameters with an intrinsic binding constant K of 5×10^8 M^{-1} and a cooperativity parameter σ of 0.06, and the empirical function defined in the text. (b) Dependence of the relative fluorescence increase, ΔF_{obs}, on the total average degree of binding of MANT-AMP-PNP to the DnaB protein, in the complex with the ssDNA oligomer, $dA(pdA)_{19}$, $\Sigma\theta_i$ (□). The values of $\Sigma\theta_i$ have been determined using the quantitative method described in Materials and Methods. The solid line is the nonlinear least-squares fit, using the empirical function defined in the text. The maximum value of the relative fluorescence increase, ΔF_{max}, is 0.45 (■).
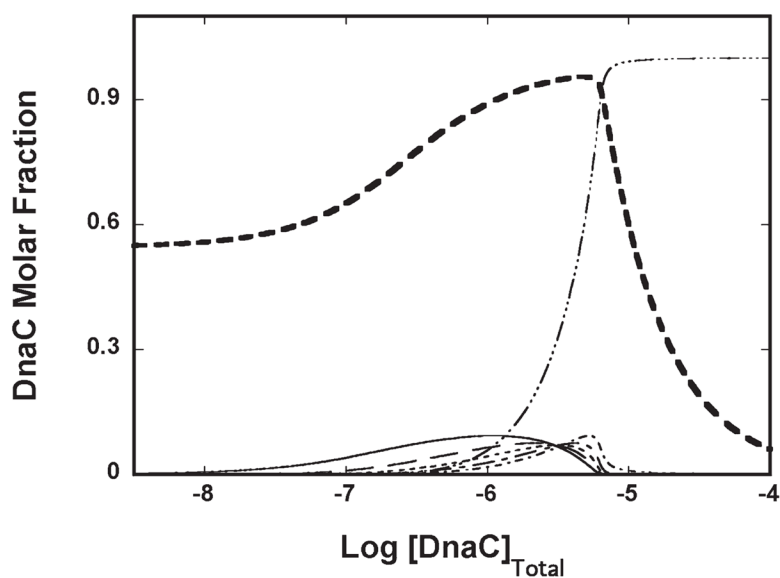
Figure 5.
(a) Fluorescence titrations of the DnaB helicase, engaged in the tertiary DnaB–DnaC–dA(pA)$_{19}$ complex, with MANT-GDP in buffer T4, at two different concentrations of the helicase: 6×10^{-7} M (■) and 1×10^{-6} M(hexamer)(□). The corresponding concentrations of the DnaC protein were 5×10^{-6} and 8×10^{-6} M, respectively. The concentration of the ssDNA 20-mer was 6.5×10^{-5} M (oligomer). The solid lines are nonlinear least-squares fits of the titration curves, according to the hexagon model (eqs 5–8) using a single set of binding parameters with an intrinsic binding constant K of 2.1×10^6 M^{-1} and a cooperativity parameter σ of 0.5. (b) Sedimentation velocity absorption profiles, recorded at 356 nm, of MANT-GDP in the presence of the tertiary DnaB–DnaC–dA(pA)$_{19}$ complex, in buffer T4. The concentrations of the DnaB and DnaC proteins were 1×10^{-6} M (hexamer) and 8×10^{-6} M, respectively. The concentrations of the ssDNA oligomer and MANT-GDP were 6.5×10^{-5} M (oligomer) and 3×10^{-5} M, respectively. The scans were collected at 25000 rpm. The short initial parts of the scans correspond to the buffer–air region above the sample meniscus. The arrows indicate the absorption of the total concentration of MANT-GDP (T), the concentration of the cofactor bound to the DnaB helicase in the DnaB–DnaC–ssDNA complex (C), and the concentration of the free MANT-GDP (F). The horizontal dashed lines indicate the locations of the plateaus corresponding the zero line, the free MANT-GDP concentration, and the total MANT-GDP concentration (see the text for details).
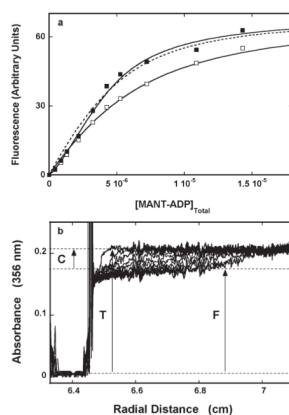
Figure 6.
Fluorescence titrations of the DnaC protein with MANT-ADP in buffer T4, at different concentrations of the ssDNA oligomer, $dA(pA)_{19}$: 0 (■), 6.5×10^{-5} M (□), and 1.2×10^{-4} M (oligomer) (▲). The solid lines are nonlinear least-squares fits of the titration curves, according to the single-site binding isotherm (eq 10), with the following binding constants: $K = 3 \times 10^5 M^{-1}$ (■), $K = 9 \times 10^5$ M^{-1} (□), and $K = 2.1 \times 10^6$ M^{-1} (▲) (see the text for details).

Figure 7.
Computer simulations of the molar fractional distribution of the DnaC–DnaB complexes, containing a different number, n, of bound DnaC protein molecules per DnaB hexamer (C_n), as a function of the total DnaC protein concentration. The simulations have been performed using the hexagon model (eqs 7 and 8) with an intrinsic binding constant K of $2 \times 10^5 M^{-1}$ and a cooperativity parameter σ of 30. The selected concentration of the DnaB protein is 1×10^{-6} M (hexamer): (__) C_1, (– – –) C_2, (—) C_3, (–––) C_4, (···) C_4, (_____) C_5, (– — –) C_6. The bold dashed line is the molar fraction contribution of the total bound DnaC protein to the total DnaC protein population, as a function of the total DnaC concentration in the sample, at the selected total DnaB concentration, defined by eq 12.
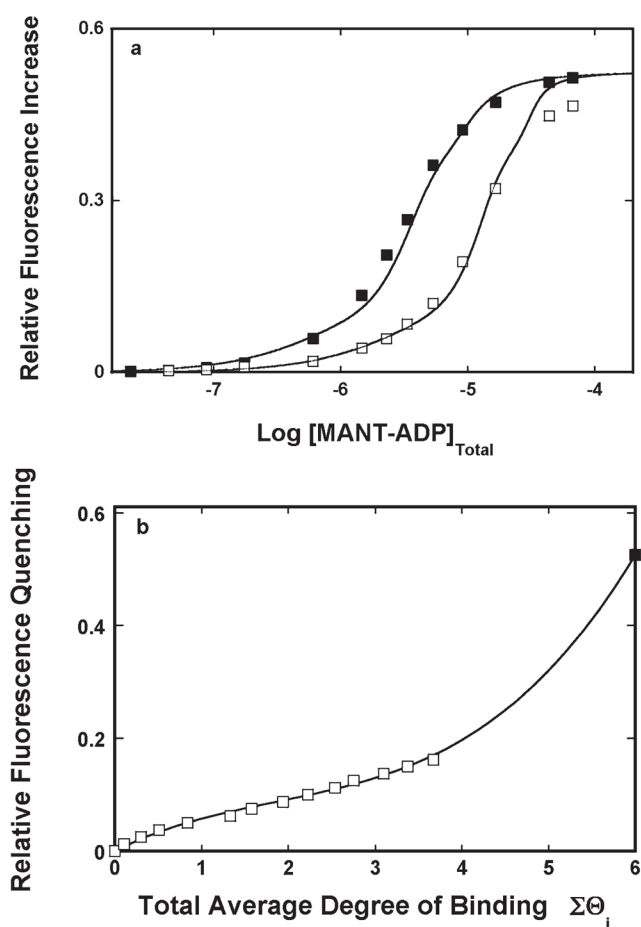
Figure 8.
(a) Fluorescence titration of the DnaC protein, engaged in the binary DnaB–DnaC complex, with MANT-ADP in buffer T4, containing 2 mM GDP (■). The concentrations of the DnaC and DnaB proteins were 5×10^{-6} M and 1×10^{-6} M (hexamer), respectively. The solid line is the nonlinear least-squares fit of the titration curve, according to the allosteric MWC model (eqs 13–15) with a binding constant K of $7.1 \times 10^5 M^{-1}$ and an allosteric constant K_A of 0.1. The dashed line is the best fit of the same titration curve, using the independent-site binding model, which treats each DnaC molecule as an independent binding unit (eq 10). For the sake of comparison, the titration of the DnaC protein, alone, at the same concentration as in the DnaB–DnaC complex is also included in the panel (□). (b) Sedimentation velocity absorption profiles at 356 nm of MANT-ADP in the presence of the binary DnaB–DnaC complex in buffer T4, containing 2 mM GDP. The concentrations of the DnaB and DnaC proteins were 1×10^{-6} M (hexamer) and 5×10^{-6} M, respectively. The concentration of MANT-GDP was 3×10^{-5} M. The scans were collected at 25000 rpm. The meanings of the symbols in the panel are the same as in the panels in Figures 2b and 4b (see the text for details).
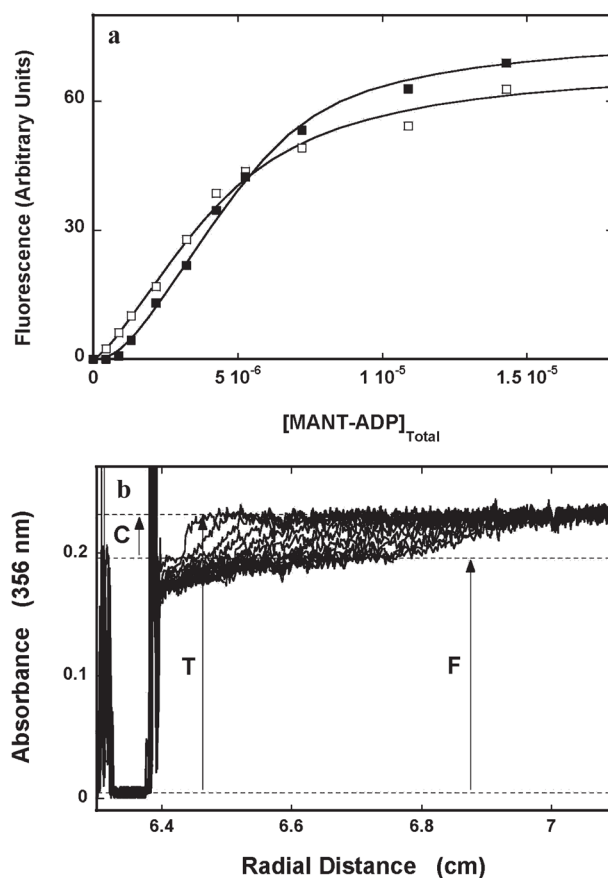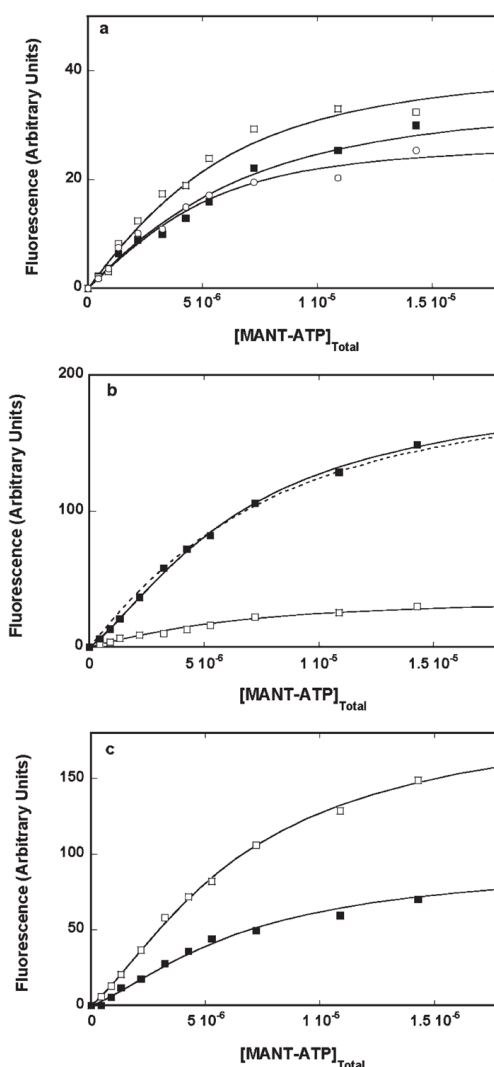
Figure 9.
(a) Fluorescence titration of the DnaC protein, engaged in the tertiary DnaB–DnaC–dA(pA)$_{19}$ complex with MANT-ADP in buffer T4, containing 2 mM GDP (■). The concentrations of the DnaC and DnaB proteins were 5×10^{-6} M and 1×10^{-6} M (hexamer), respectively. The concentration of the ssDNA 20-mer was 6.5×10^{-5} M (oligomer). The solid line is the nonlinear least-squares fit of the titration curve, according to the allosteric MWC model (eqs 13–15) with a binding constant K of $7.9 \times 10^5 M^{-1}$ and an allosteric constant K_A of 0.005. For the sake of comparison, the titration of the DnaC protein in the binary DnaB–DnaC complex, at the same concentration as in the tertiary complex, is also included (□). (b) Sedimentation velocity absorption profiles recorded at 356 nm of MANT-ADP in the presence of the tertiary DnaB–DnaC–dA (pA)$_{19}$ complex, in buffer T4, containing 2 mM GDP. The concentrations of the DnaB and DnaC proteins were 1×10^{-6} M (hexamer) and 5×10^{-6} M, respectively. The concentrations of dA(pA)$_{19}$ and MANT-GDP were 6.5×10^{-5} M (oligomer) and 3×10^{-5} M, respectively. The scans were collected at 25000 rpm. The meanings of the symbols in the panel are the same as in Figures 2b and 4b (see the text for details).
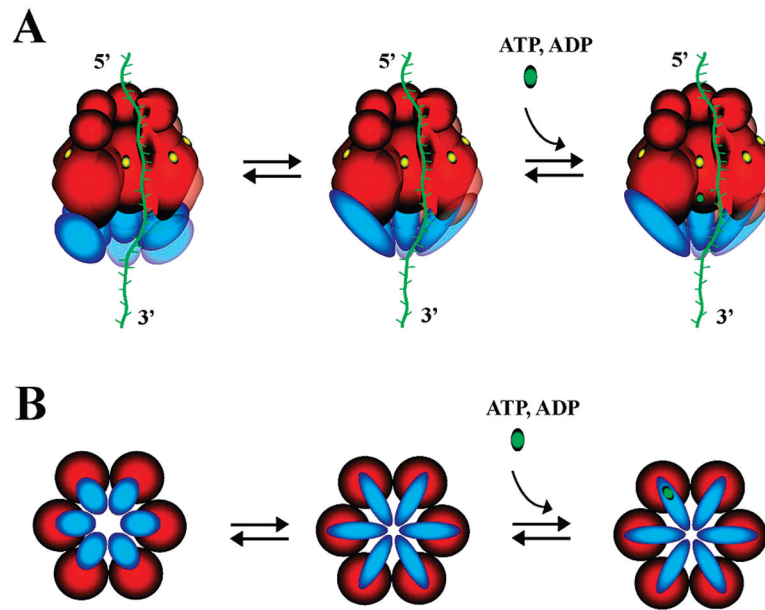
Figure 10.
(a) Fluorescence titrations of the tertiary DnaB–DnaC–dA(pA)$_{19}$ complex with MANT-ADP in buffer T4. The concentrations of the DnaC and DnaB proteins were 5×10^{-7} and 8×10^{-6} M (■), respectively, and 2×10^{-6} M(hexamer) and 2×10^{-5} M (□), respectively. The concentration of the ssDNA 20-mer was 6.5×10^{-5} M (oligomer). The solid lines are nonlinear least-squares fits of the titration curves, according to eqs 16–20, using a single set of binding parameters, with an intrinsic binding constant K of 5×10^{8} M^{-1} and a cooperativity parameter σ of 0.06, and the empirical function defined in the text. (b) Dependence of the relative fluorescence increase, ΔF_{obs}, on the total average degree of binding of MANT-ADP to the DnaB protein, $\Sigma \theta_i$, in the tertiary DnaB–DnaC–dA(pA)$_{19}$ complex (□). The values of $\Sigma \theta_i$ have been determined using the quantitative method described in Materials and Methods. The solid line is the nonlinear least-squares fit, using the empirical function defined in the text. The maximum value of the relative fluorescence increase, ΔF_{max}, is 0.52 (■).

Figure 11.
(a) Fluorescence titrations of the DnaC protein with MANT-ATP in buffer T4, at different concentrations of the ssDNA oligomer, dA(pA)$_{19}$: 0 (■), 6.5×10^{-5} M (□), and 1.2×10^{-4} M (oligomer) (○). The solid lines are nonlinear least-squares fits of the titration curves, according to the single-site binding isotherm (eq 10), with the following binding constants: $K = 3 \times 10^5 M^{-1}$ (■), $K = 4 \times 10^5$ M^{-1} (□), and $K = 6 \times 10^5$ M^{-1} (○) (see the text for details). (b) Fluorescence titration of the DnaC protein, engaged in the binary DnaB–DnaC complex with MANT-ATP in buffer T4, containing 2 mM GDP(■). The concentrations of the DnaC and DnaB proteins were 5×10^{-6} M and 1×10^{-6} M (hexamer), respectively. The solid line is the nonlinear least-squares fit of the titration curve, according to the allosteric MWC model (eqs 13–15) with a binding constant K of $2.4 \times 10^5 M^{-1}$ and an allosteric constant K_A of 0.6. The dashed line is the best fit of the same titration curve, using the independent-site binding model, which treats each DnaC molecule as an independent binding unit with a binding constant K of $2.2 \times 10^5 M^{-1}$ (eq 10). For the sake of comparison, the titration of the DnaC protein alone, at the same concentration as in the DnaB–DnaC complex, is also included (□). (c) Fluorescence titration of the DnaC protein, engaged in the tertiary DnaB–DnaC–dA(pA)$_{19}$ complex, with MANT-ATP in buffer T4, containing 2 mM GDP (■). The concentrations of the DnaC and DnaB proteins were 5×10^{-6} M and 1×10^{-6} M (hexamer),

respectively. The concentration of the ssDNA 20-mer was 6.5×10^{-5} M (oligomer). The solid line is the nonlinear least-squares fit of the titration curve, according to the allosteric MWC model (eqs 13–15)with a binding constant K of $2.4 \times 10^5 M^{-1}$ and an allosteric constant K_A of 0.5. For the sake of comparison, the titration of the DnaC protein in the binary DnaB–DnaC complex, at the same concentration as in the tertiary complex, is also included (□).

Figure 12.
Schematic representation of the allosteric transition of the six DnaC protein molecules bound to the DnaB hexamer in the tertiary DnaB–DnaC–ssDNA complex based on the thermodynamic data described in this work (A). The DnaB helicase preferentially, but not exclusively, binds the DnaC protein in the conformation that does not possess nucleotide binding capability. Consequently, the binary DnaB–DnaC or tertiary DnaB–DnaC–ssDNA complex, with six DnaC molecules, assembled as a hexamer on the DnaB protein, also exits in solution in an equilibrium between two conformations of the assembled DnaC hexamer, with only one conformation of the DnaC protein able to bind nucleotide cofactors. Thus, the DnaC hexamer, assembled on the DnaB helicase, forms an allosteric cooperative system. Binding of a single nucleotide cofactor to one of the bound DnaC molecules induces the transition of the entire assembled DnaC hexamer to the conformation that has significant affinity for the nucleotide cofactor. Because the DnaC protein exclusively binds adenosine nucleotides, the allosteric transition of the DnaB–DnaC complex is exclusively induced by ATP or ADP binding (56). Panel B shows the global conformational transitions of the DnaC hexamer, assembled on the DnaB helicase, in the absence and presence of the bound nucleotide, as obtained in hydrodynamic and spectroscopic studies of the protein (30).